INORGANIC CHEMISTRY
FRONTIERS

RESEARCH ARTICLE

View Article Online
View Journal | View Issue

Cite this: *Inorg. Chem. Front.*, 2021, **8**, 1015

Copper catalysts for photo- and electro-catalytic hydrogen production†

Abdullah M. Abudayyeh,[a] Olivier Schott,[b] Humphrey L. C. Feltham,[a] Garry S. Hanan *[b] and Sally Brooker *[a]

Green production of hydrogen, a carbon-zero future fuel, requires long lived, high activity catalysts made from inexpensive, earth abundant metal ions. Only 15 molecular copper complexes catalyze the H_2 evolving reaction (HER). Herein 3 such complexes are prepared and studied as catalysts for both photo- and electro-catalytic HER. Two new N_5-donor analogues of the literature N_4-donor Schiff base macrocycle HL^{Et} (from [1 + 1] condensation of 2,2′-iminobisbenzaldehyde (**dpa**) and diethylenetriamine), macrocycle $HL^{Et\text{-}MePy}$ (2-bromomethylpyridine alkylation of HL^{Et}) and non-cyclic HL^{EtPy2} (condensation of **dpa** and two 2-aminoethylpyridine), were prepared. Then literature $[Cu^{II}(L^{Et})]BF_4$ (**1**), and new $[Cu^{II}(L^{Et\text{-}MePy})]BF_4$ (**2**) and $[Cu^{II}(L^{EtPy2})]BF_4$ (**3**), were prepared and structurally characterized, revealing square, square pyramidal and trigonal bipyramidal copper(II) geometries, respectively. Testing under photocatalytic conditions showed that **1–3** have modest turnover numbers (TON = 460–620), but the control, using $Cu(BF_4)_2$, had a higher TON (740), and the blank (no copper) also had significant activity (TON_{equiv} = 290). So this is a cautionary tale: whilst **1–3** initially appeared to be promising catalysts for photocatalytic HER, running the control and blank – studies often not reported – shows otherwise. Hence the focus shifted to electrocatalytic HER testing. All three complexes show reversible redox events in MeCN *vs.* 0.01 M $AgNO_3$/Ag: $E_{1/2}$ = –1.39 V (**1** and **2**); –0.89 V (**3**). Unlike complexes **2** and **3** or the control, **1** is shown to be, or to form, an effective and stable electrocatalyst for HER in MeCN with acetic acid as the proton source (at 100 mV s^{-1}, $E_{cat/2}$ = –1.64 V so overpotential necessary for catalysis = 0.23 V, and i_{cat}/i_p = 34, where i_{cat} is peak catalytic current and i_p is $1e^-$ peak current for **1** in absence of acid): after 6 hours at –1.6 V, the TON for **1** is 12.5, despite the tiny glassy carbon working electrode used, and it retains good electrocatalytic activity. Results of both 'rinse and repeat' (for catalytically active deposit on working electrode) and drop of Hg (for formation of catalytically active nanoparticles) tests are consistent with homogeneous catalysis by **1**, but a small copper stripping wave is seen after acetic acid is added, so it is probable that these initial test results are 'false negatives', and that there is a heterogenous catalytically active species present; so future studies will probe this point further.

Received 15th October 2020,
Accepted 10th December 2020

DOI: 10.1039/d0qi01247e

rsc.li/frontiers-inorganic

Introduction

There are many acute global challenges which have the potential for unprecedented adverse impacts on human health and global ecosystems.[1] These include climate change, exceptional wild fires, and ocean acidification – which are to a great extent due to the ongoing large scale combustion of fossil fuels, as this leads to ever increasing concentrations of greenhouse gases such as CO_2 in the atmosphere.[2] Therefore the development of carbon neutral (circular or closed carbon cycles), or better still carbon zero (H_2) future fuels with production driven by green energy (renewables, such as solar, wind or wave generated energy) sources is an urgent necessity.[3]

One of the most attractive strategies to achieve this aim is to mimic plants and store light energy in chemical bonds, forming so called 'solar fuels', such as hydrogen.[4–6] Hydrogen is particularly attractive because it is a carbon zero fuel (produces only water and energy on combustion) and has a higher energy density than fossil fuels[7] and batteries.[8,9] Current commercial production of hydrogen uses a platinum catalyst, but for hydrogen to be widely adopted, it is essential that active long-lived new catalysts based on cheap, abundant metals be developed.[10]

[a]*Department of Chemistry and the MacDiarmid Institute for Advanced Materials and Nanotechnology, University of Otago, PO Box 56, Dunedin 9054, New Zealand. E-mail: sbrooker@chemistry.otago.ac.nz; Fax: +64-3-4797906; Tel: +64-3-479 7912*
[b]*Département de Chimie, Université de Montréal, Montréal, Quebec H3T 1J4, Canada*

†Electronic supplementary information (ESI) available: Additional synthetic, crystallographic, photo- and electro-catalytic HER data and figures, as well as NMR and mass spectra. CCDC 1983967 1983968. For ESI and crystallographic data in CIF or other electronic format see DOI: 10.1039/d0qi01247e

Over the last few decades, various earth-abundant molecular cobalt,[11–17] iron and nickel[18,19] catalysts have exhibited activity for HER under photocatalytic conditions. Several very useful reviews of photochemical HER using earth-abundant molecular catalysts have been presented, and confirm that only 3 are based on copper.[20–24] This is perhaps surprising, as copper complexes have well determined coordination chemistry, as well as rich redox and photo-chemistry, and are well known as catalysts in several other types of transformations,[25–34] including CO_2 reduction[29] and water oxidation.[30–34] But copper-based molecular catalysts have an enhanced propensity, under reducing conditions in the presence of water, to breakdown and form heterogeneous reduction products,[35,36] such as metallic nanoparticles or deposits on the working electrodes, which can be active HER electrocatalysts in their own right.[37–41] This fact may well have discouraged researchers from working with molecular copper catalysts for HER. But careful testing for the possible degradation of the molecular copper catalyst to form nanoparticles (mercury drop test or DLS) or deposits on the working electrode (rinse and repeat test, SEM/XPS) can, and should, be done, to help rule these out.[42,43]

To date, only 15 copper complexes (Fig. 1) have been reported to be active as molecular catalysts for HER:[42,44–53] 14 are active HER electrocatalysts,[42,44–53] and 3 (Fig. 1, box) are active catalysts for light-driven HER.[48,51]

Considering electrocatalysis first: the first molecular copper catalyst for HER, **A**, was supported by an N_5-donor extended tripodal ligand, and was reported in 2014 by Wang, Sun and co-workers.[42] Complex **A** exhibited a turnover frequency (TOF) of 7000 h^{-1} cm^{-2} in water (*i.e.* TOF per electrode surface area). Then Zhan and co-workers reported copper(II) complexes a pair of mononuclear salen-like ligands (N_2O_2-donor), **B1** & **B2**,[45,46,54] as well as one tri- and two dinuclear copper complexes of bis-triazenido-type ligands (bridging N_2 donor), **C1–C3**,[47,52,53] all 5 of which were active HER electrocatalysts in water.[45–47] Catalysts **B1** & **B2** had faradaic efficiencies of 91–96% and TOFs of up to 1331.7 h^{-1}.[45,46] Copper(I) complexes **C1** & **C2**, and copper(II) complex **C3**, were active electrocatalysts in water, when acetic acid (AcOH) was used as the proton source, at overpotentials of 789–942 mV (applied potentials of −1.45 to −1.47 V *vs.* Ag/AgCl) with faradaic efficiencies of 94–97%.[52,53] In the same year, Lai, Fu, Cao and co-workers reported that several copper(II) corroles (N_4-donor macrocycle), **D1–D4**, were active electrocatalysts for HER, with the best of them, **D1** & **D2**, featuring electron withdrawing groups on the *meso* positions of the corrole macrocycle, and an i_{cat}/i_p of 303, (where i_{cat} is the maximum catalytic current and i_p is the peak current in the absence of acid) in acetonitrile with trifluoroacetic acid (TFA) as the proton source.[44]

The pair of known copper complexes of a tripodal ligand, copper(II) chloride **H1** & copper(II) dichloride **H2**,[55,56] were subsequently examined, in 2016, by Hou, Wang and co-workers and found to exhibit electrocatalytic HER in acetonitrile, with acetic acid as the proton source, when −1.8 V *vs.* SCE was applied, yielding a faradaic efficiency of ~95%.[48] In 2017,

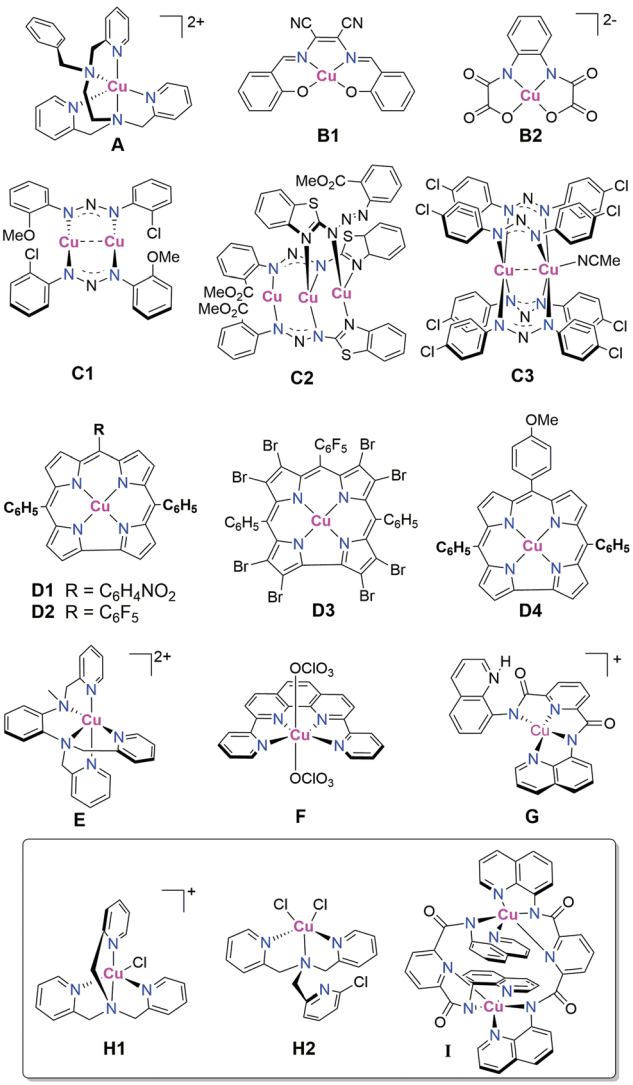

Fig. 1 The 15 copper-based molecular catalysts reported to date to be active for HER;[42,44–53] 14 of which (all except I) are active electrocatalysts,[42,44–53] whilst the box contains the 3 that are active under photocatalytic conditions.[48,51]

probably inspired by **A**, the copper(II) complex of a slightly different extended tripodal N_5-donor ligand, **E**, was reported by Mazumder, Verani and co-workers to exhibit electrocatalytic HER in water at pH 2.5, with a TON of 3900 mol H_2 per mol of catalyst over 3 hours at −1.7 V *vs.* Ag/AgCl using a Hg pool working electrode, with no evidence of electrodeposition.[49] Also in 2017, the water-soluble perchlorate salt of the copper(II) complex of an N_4-donor pyridine-phen-pyridine ligand, **F**, prepared by Wang and co-workers, was reported to electrocatalyse HER in neutral water (phosphate buffer; SHE reference electrode) when held at an overpotential of 520 mV. A TON of 734 mol H_2 per mol of catalyst was recorded over 2 hours.[50] Finally, also in 2017, Padhi and co-workers reported that a mononuclear copper(II) complex of a dianionic N_4-donor ligand, **G**, displayed HER electrocatalytic activity in 95 : 5 DMF/H_2O (v/v) in the presence of acetic acid as the proton source, at

−1.6 V *vs.* SCE (saturated calomel electrode) with i_{cat}/i_p = 24 and TOF of ~112 s^{-1}.[51]

Turning now to the 3 molecular copper catalysts shown to date to be active for HER under photocatalytic conditions: in 2016 Hou, Wang and co-workers showed that the two tripodal copper complexes **H1** & **H2** were active not only as HER electrocatalysts (see above), but that they were also the first examples of copper based molecular catalysts to be active under *photocatalytic* HER conditions.[48] By using a relatively low concentration of catalyst (1 μM), high TONs, of 6108 and 10 014 over 6 hours, were achieved for the copper(II) monochloride (**H1**) and copper(II) dichloride (**H2**), respectively, when driven by visible irradiation (λ = 400 nm; violet) with an Ir based photosensitizer (PS) (0.2 mM), in 9 : 1 MeCN/H_2O (v/v), using triethylamine (TEA) as sacrificial reductant.[48] Then in 2017, Padhi and co-workers demonstrated that visible light irradiation of the doubly μ-pyridine-bridged dicopper(II) complex **I** enabled HER in 80 : 20 DMF : H_2O solution using fluorescein as PS, and TEA as sacrificial reductant, with a maximum TOF of 0.03 s^{-1}. They also showed that, once it had plateaued, some of the activity of the system was restored on the addition of fresh catalyst, indicating that it is the lifetime of the catalyst, not the PS, that is the limiting factor.[51]

Of the above 15 molecular copper HER catalysts, testing to help rule out the presence of nanoparticles (either Hg drop or DLS), and/or the presence of a deposit on the working electrode (rinse and repeat, or SEM/XPS), was carried out in most, but not all, of the reported cases. These tests were used to try and help rule out heterogeneous catalysis in the case of the electrocatalysts **A**,[42] **B2**,[46] **D**,[44] **E**,[49] **F**,[50] and **G**,[51] although in the case of **E** some decomposition was observed after 8 hours of electrolysis.[49] No nanoparticle or other heterogeneous deposit testing was done for the photocatalysts, **H1** and **H2**,[48] or **I** (despite evidence of degradation of **I** during photocatalysis).[51] Clearly, the results of these tests should always be reported for molecular copper HER catalysts. But it is also critically important to point out that these tests are insufficient to rule out such heterogeneous species being the actual active catalytic species. Artero and co-workers reported a particularly comprehensive illustration of this in 2016, in which the active catalyst is not the molecular complex but is the heterogeneous deposit formed. But as the latter was meta-stable and readily redissolved before the rinse and repeat test, this led to a 'false negative' test result.[57] Dempsey and co-workers have recently written a superb tutorial review on this issue.[58]

We recently reported[16] that 17 cobalt complexes of a wide range of polydentate and macrocyclic ligands were effective catalysts for HER under photocatalytic conditions. The best of them, $[CoL^{Et}]^+$, was supported by an anionic N_4-donor macrocycle (Fig. 2) and had a TON of 26, *vs.* TON(cobaloxime) of 9, both determined in DMF, with $[Ru(bpy)_3]^{2+}$ as the PS and triethanolamine (TEOA) as the proton source, under blue light irradiation.

Herein the analogous *copper* complex, $[Cu^{II}(L^{Et})]BF_4$ (**1**, Fig. 2), of that N_4-donor macrocycle, as well as two new copper complexes of two new N_5-donor ligands that are prepared

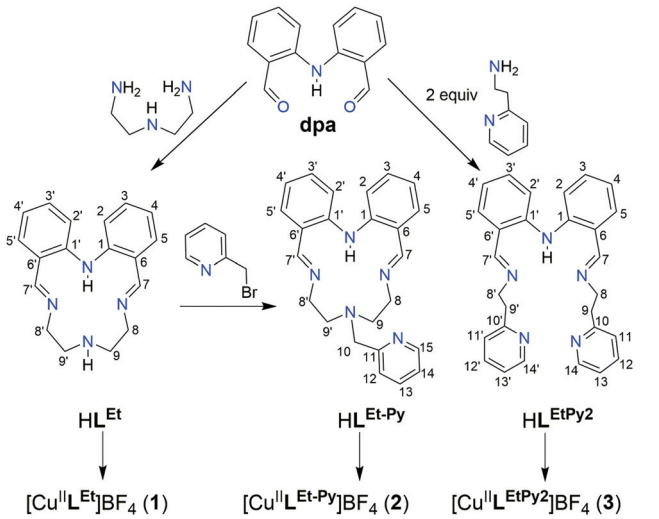

Fig. 2 Synthesis of the three Schiff-base ligands, two macrocyclic (literature HL^{Et},[59,60] and new $HL^{Et\text{-}MePy}$) and one new acyclic (HL^{EtPy2}) ligand, from which the three copper(II) complexes (**1–3**) were prepared by 1 : 1 : 1 reaction of ligand to TEA to $Cu^{II}(BF_4)_2{\cdot}H_2O$.

herein (Fig. 2), macrocyclic $[Cu^{II}(L^{Et\text{-}MePy})]BF_4$ (**2**) and acyclic $[Cu^{II}(L^{EtPy2})]BF_4$ (**3**), are tested for HER activity – as we look to grow the number of copper-based molecular HER catalysts. All 3 are shown to be active HER catalysts under photocatalytic conditions, despite presenting differing copper coordination geometries: square (**1**), square pyramidal (**2**) and trigonal bipyramidal (**3**). These findings double the number of known molecular copper catalysts for photocatalytic HER (only 3 prior examples; Fig. 1, box). But, disappointingly, on running the appropriate control and blank tests – not reported for the previous copper HER catalysts in the literature – these complexes are revealed to be no more active than the simple salt copper (II) tetrafluoroborate under photocatalytic conditions. This highlights the importance of always doing, and reporting, the results of blanks and controls, in order to put the observed activity of the complexes studied into proper context. In light of the disappointing photocatalysis results, our attention turned to the potential of **1–3** as electrocatalysts for HER. Pleasingly, all 3 complexes exhibit reversible redox processes in MeCN ($E_{1/2}$ = −0.89 to −1.39 V *vs.* 0.01 M $AgNO_3$/Ag). Even better is that in electrocatalysis tests on **1**, in MeCN with acetic acid as the proton source, the electrocatalytic HER activity is retained for more than 6 hours.

Results and discussion

Ligand synthesis

The Schiff-base macrocycle HL^{Et} was prepared, from 2,2′-iminobisbenzaldehyde (**dpa**) and diethylenetriamine, using the literature procedure (Fig. 1).[59,60]

This N_4-donor HL^{Et} macrocycle was then converted into the N_5-donor analogue, $HL^{Et\text{-}MePy}$ (Fig. 2), by adding a methylpyridyl 'arm'; *via N*-alkylation with 2-(bromomethyl)pyridine in

dry THF at room temperature in the presence of excess triethylamine (TEA). The desired ligand was obtained as $HL^{Et\text{-}MePy}$·0.5DCM, according to both elemental analysis and the relative integration of the solvent peak in the ^{1}H NMR spectrum of this red solid, in 63% yield. The third ligand, the N_5-donor *non-cyclic* Schiff base ligand analogue, HL^{EtPy2} (Fig. 2), was prepared by condensation of **dpa** with 2 equivalents of 2-aminoethylpyridine in refluxing acetonitrile, in quantitative yield, as HL^{EtPy2}·0.25$(CH_3)_2CO$, according to both elemental analysis and the relative integration of the solvent peak in the ^{1}H NMR spectrum of this sticky red oil.

Synthesis of complexes

A metal templated cyclisation of **dpa** and diethylenetriamine was employed to prepare $[Cu^{II}(L^{Et})]BF_4$ (**1**) in the literature,[59] but unsurprisingly it is shown herein that it can also be prepared by metalation of the pre-formed macrocycle, as has been previously reported for other 3d metal complexes of this macrocycle.[59]

All three complexes, **1–3**, were prepared by 1 : 1 : 1 reaction of the appropriate ligand (HL^{Et}, $HL^{Et\text{-}MePy}$ and HL^{EtPy2}) with TEA and $Cu^{II}(BF_4)_2$·H_2O. In all cases an instantaneous change in colour from yellow to dark red occurs on adding the copper salt. Dark orange crystals of complex **1** and dark red needles of complexes **2** and **3**, suitable for single crystal X-ray structure determinations (see below), were grown by diethylether vapour diffusion into the reaction solutions. The complexes were pure by elemental analysis and were further characterized by electrospray mass spectrometry (ESI-MS), UV-vis spectroscopy and single crystal X-ray structure determinations. All three complexes, **1–3**, are soluble in most common solvents: they are highly soluble in methanol, acetonitrile and DMF, and have moderate solubility in dichloromethane, chloroform and water.

The ESI-MS spectra of **1–3** all showed an intense peak attributed to the respective monocation: $[Cu(L^{Et})]^+$ at m/z = 354.0902, $[Cu(L^{Et\text{-}MePy})]^+$ at 445.1310 and $[Cu(L^{EtPy2})]^+$ at 495.1451.

UV-vis spectra were obtained on **1–3** in DMF (300–1200 nm, Fig. 3). All feature two intense absorptions at low wavelengths, in the range 334–336 nm (ε = 3793–5733 M^{-1} cm^{-1}) and 399–408 nm (ε = 3313–5371 M^{-1} cm^{-1}), as well as a much more intense absorption in the visible, 466–491 nm (ε = 6216–13 500 M^{-1} cm^{-1}). Small red shifts of the most intense band, from 466 nm for the complex of the N_4-donor macrocycle, **1**, are seen for the complexes of the two N_5-donor ligands, by +13 nm for **2** and by +23 nm for **3**.

In all three cases a d–d band is also clearly seen: at 672 (453) for **1**, 789 (342) for **2** and 917 nm (309 M^{-1} cm^{-1}) for **3**. Hathaway[61] established that in general d–d transitions in copper(II) complexes that are square planar N_4-coordinated occur at higher energy than for those that are square pyramidal N_5-coordinated, which in turn occur at a higher energy than for trigonal bipyramidal analogues.[62,63] This is in excellent agreement with the present findings: 14 881 cm^{-1} (square planar **1**) > 12 674 cm^{-1} (square pyramidal **2**) > 10 905 cm^{-1} (trigonal bipyramidal **3**).

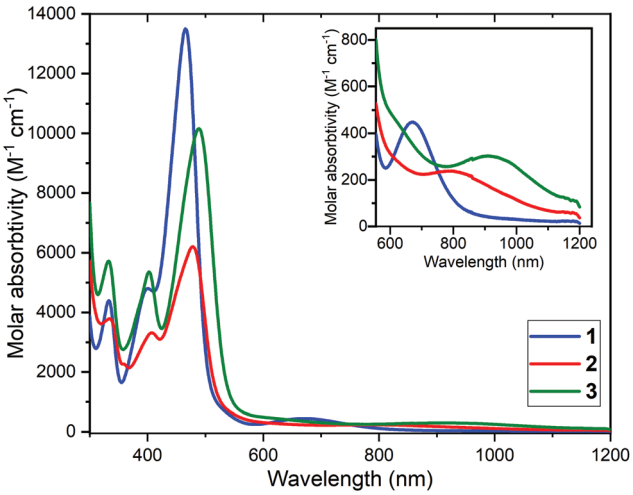

Fig. 3 UV-vis spectra of 0.21 mM DMF solutions of: $[Cu^{II}L^{Et}](BF_4)$ (**1**) blue line; $[Cu^{II}L^{Et\text{-}MePy}](BF_4)$ (**2**) red line; $[Cu^{II}L^{EtPy2}](BF_4)$·0.5H_2O (**3**·0.5H_2O) green line. Inset: Expansion of 600–1200 cm^{-1} region.

Structures of complexes

As reported earlier,[59] complex **1** features a *square planar* (τ_4 = 0.01)[64] copper(II) center with 4N donors, comprising the deprotonated diphenylamine, two imines and the tertiary amine (Fig. 4 top and Table 1).

Herein, X-ray structure determinations are reported for complexes **2** and **3** (Fig. 4 and Table 1), for which the asymmetric unit comprised the entire cationic complex and a tetrafluoroborate anion. The Cu(II) center in the pyridyl-armed macrocycle, **2**, is distorted *square pyramidal* (τ_5 = 0.27; *vs.* 0 for a perfect square pyramid)[65] through the addition of the axially coordinated pyridyl arm (Fig. 4, middle). In contrast, in the non-cyclic analogue complex **3** the Cu(II) center adopts a distorted *trigonal bipyramidal* geometry (τ_5 = 0.83; *vs.* 1 for a perfect trigonal bipyramid)[65] with the trigonal plane comprising the nitrogen donors from the deprotonated diphenylamine and two pyridine arms, and the two imine nitrogen atoms coordinating axially (Fig. 4, bottom).

The Cu–N bond lengths in **1–3** are interesting. In the square-based complexes, **1** and **2**, the two imine nitrogen atoms are bound asymmetrically to the copper centre. As a result, one $Cu\text{–}N_{imine}$ bond is the shortest Cu–N bond in the complex (**1**, 1.898(6); **2**, 1.939(4) Å), followed by the $Cu\text{–}N_{dpa}$ bond length (**1**, 1.932(6); **2**, 1.940(6) Å), whilst the other $Cu\text{–}N_{imine}$ bond is either the same length (**1**, 1.932(5) Å) or slightly longer again (**2**, 1.944(7) Å) than the $Cu\text{–}N_{dpa}$ bond (Table 1). In both cases the longest bond is the $Cu\text{–}N_{amine}$ bond (**1**, 2.036 (6); **2**, 2.106(5) Å). The situation for the *noncyclic* complex, **3**, is quite different from that in the *cyclic* complexes **1** and **2**: the $Cu\text{–}N_{imine}$ bonds are far closer to symmetrical, the $Cu\text{–}N_{dpa}$ bond is the shortest, and the two axial $Cu\text{–}N_{pyridine}$ bonds are easily the longest (Table 1). As expected, the average Cu–N

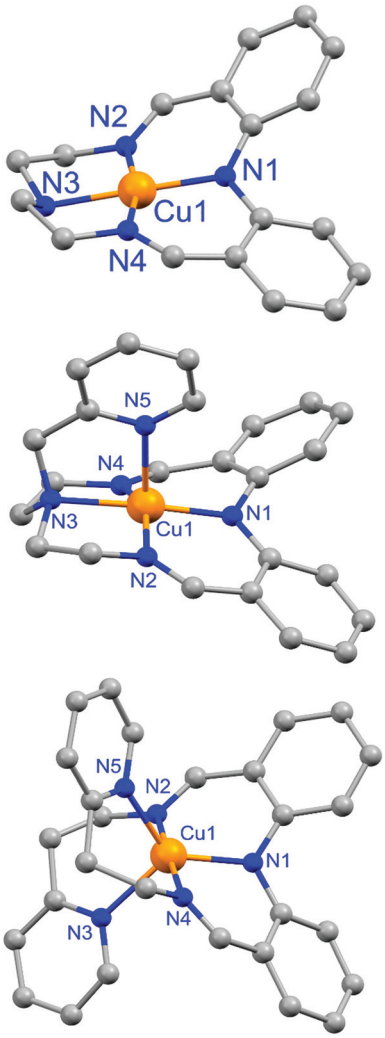

Fig. 4 X-ray crystal structures (shown as ball and stick diagrams) of the monocations of (from top to bottom): macrocyclic complexes **1** (square planar Cu^{II}) and **2** (square pyramidal Cu^{II}), and non-cyclic complex **3** (trigonal bipyramidal Cu^{II}).

bond length increases on going from 4-coordinate (1.950 Å) to 5-coordinate (square pyramidal 2.035; trigonal bipyramidal 2.066 Å).

Photocatalytic hydrogen evolution

All experiments were conducted on a 5 mL DMF solution containing: 5 μM catalyst, 1 M triethanolamine (TEOA) as the sacrificial reductant, 0.2 mM $[Ru(bpy)_3](PF_6)_2$ (bpy = 2,2′-bipyridyl) as the photosensitizer (PS), and 0.1 M (2.8 mL HBF_4 (aq) 48% w/w dissolved in 100 mL DMF) as the proton donor, under irradiation by a blue LED (λ = 445 nm, 88 mW cm^{-2}) at 20 °C (Fig. 5, 6 and Tables 2, 3). Blanks and controls were run under identical conditions but with the omission of either the catalyst or PS or LED irradiation, or replacement of the copper complex with the simple salt copper(II) tetrafluoroborate. No hydrogen evolution was seen in the absence of PS or of LED irradiation; the other results are discussed below (Fig. S2–S6†). Multiple tests were run for all of the complexes and average values of turnover number (TON), maximum turnover frequency (TOF) and volume of H_2 produced are given in Table 2.

All three complexes, **1–3**, are active for HER under photochemical conditions (Fig. 5 and Table 2), with approximately 11.4–15.5 μmol of hydrogen produced over 5 hours of blue light LED irradiation (Fig. 5). The corresponding TON values (mol of H_2/mol of catalyst) increased from 460 for square pyramidal copper complex **2** to 560 for non-cyclic trigonal bipyramidal complex **3** to 620 for square planar **1** (Fig. 5 and Table 2). Comparison of these TON values to those of the only 3 molecular copper catalysts previously reported to be active for photocatalytic HER (Fig. 1), reveals that **H1** and **H2** had much higher TONs (6108 and 10 014), albeit measured at 5 times lower catalyst concentration (1 μM) than herein, and using an Ir–PS.[48] No TON was reported for the third such copper catalyst **I**.[51]

The blank test with no copper catalyst present produced an average of about half of that amount of hydrogen (7.2 μmol, TON = 290; Fig. 5, Table 2 and Fig. S16†). Disappointingly, control tests using a simple salt, $Cu^{II}(BF_4)_2$ or $Cu^{II}(NO_3)_2$, as the catalyst (Fig. 5, Table 2 and Fig. S7†) produced slightly more hydrogen (18.5 and 17.9 μmol, TON 740 and 720, respectively) than the copper complexes did. Eisenberg and co-workers have previously reported that the simple salt $Ni(NO_3)_2$, used as a control during photocatalytic HER testing in aqueous media, was highly active,[66] and during the writing of this manuscript Wang, Fu and co-workers reported that $CuSO_4$ in basic aqueous solution under photocatalytic conditions can form Cu_2O and Cu nanoparticles that are active HER catalysts.[41] But to the best of our knowledge no one has reported a simple copper salt control experiment in non-aqueous photocatalytic conditions prior to our report herein.

The trend in maximum turnover frequency (TOF_{max}/min^{-1}) follows the same order at the TON values: 12 for square pyramidal **2** < 16 for non-cyclic trigonal bipyramidal **3** and square planar **1** < 24–26 for the simple copper salts (Table 2, see Fig. S8 of ESI† for TOF plot). In all cases this maximum occurred within 5–11 minutes of turning on the blue LED. A half-life, the time taken for this activity to drop by 50%, can be calculated (see ESI, Fig. S9–S12†) and is in the range 13–24 minutes for **1–3**, and 17 minutes for the BF_4 salt.

In an attempt to reactivate the system and thereby test whether the loss of activity was caused at least in part by decomposition of the PS, a fresh 1.25 mL aliquot of PS solution (same aliquot as added initially) was added to the test solutions of complexes **1**, **2** and **3**, and of the controls, after 5 hours of irradiation. In all cases this results in a partial recovery of the activity of the photocatalytic system (Fig. 6, Table 3 and Fig. S19–S21†). The total hydrogen produced over a further 10 hours, increased: 6.7 μmol for **2** to 7.6 μmol for **3** to 7.8 μmol for **1**, which corresponds to restoration of 49–53% of the original activity. In the same way, restoration of the activity of the blank (no copper catalyst) and control (simple copper salt) was tested (Fig. 6, Table 3 and Fig. S18†), and found to restore 31–33% of the original activity, generating 2.5

Table 1 Selected bond lengths [Å] and angles [°] for the literature square planar complex $[Cu^{II}L^{Et}]BF_4$ (**1**),[59] as well as for the new square pyramidal $[Cu^{II}L^{Et\text{-}MePy}](BF_4)$ (**2**) and trigonal bipyramidal $[Cu^{II}L^{EtPy2}](BF_4)$ (**3**) complexes (see also Tables S5–S8†)

	$[Cu^{II}L^{Et}](BF_4)$ 159	$[Cu^{II}L^{Et\text{-}MePy}](BF_4)$ 2	$[Cu^{II}L^{EtPy2}](BF_4)$ 3
Coordination	N_4 – square planar	N_5 – square pyramidal	N_5 – trigonal bipyramidal
Distortion parameter	$\tau_4 = 0.01^a$	$\tau_5 = 0.27^b$	$\tau_5 = 0.83^b$
$Cu(1)–N(1)_{dpa}$	1.932(5)	1.940(6)	1.975(3)
$Cu(1)–N(2)_{imine}$	1.932(6)	1.944(7)	1.992(3)
$Cu(1)–N(4)_{imine}$	1.898(6)	1.939(4)	1.984(3)
$Cu(1)–N(3)_{amine\ or\ pyridine}$	2.036(6) amine	2.106(4) amine	2.206(3) pyridine
$Cu(1)–N(5)_{pyridine}$	—	2.247(4)	2.173(3)
Average Cu–N	1.950	2.035	2.066
N(2)–Cu(1)–N(1)	96.4(2)	94.7(3)	89.1(1)
N(2)–Cu(1)–N(4)	166.2(2)	157.9(3)	178.4(2)
N(1)–Cu(1)–N(4)	96.1(2)	94.9(1)	89.4(1)
N(1)–Cu(1)–N(3)	179.3(3)	174.4(3)	123.9(1)
N(4)–Cu(1)–N(3)	84.0(2)	85.1(3)	90.7(1)
N(2)–Cu(1)–N(3)	83.6(2)	83.5(2)	90.3(1)
N(1)–Cu(1)–N(5)	—	104.6(2)	128.4(2)
Range *cis* N_{eq}–Cu–N_{eq} [c]	83.6–96.4	83.5–94.9	107.7–128.4
Range *trans*-N–Cu–N	166.3, 179.3[d]	157.9, 174.4[d]	178.4[e]

[a] 4-Coordinate distortion parameter τ_4 (0 = square planar; 1 = tetrahedral).[64] [b] 5-Coordinate distortion parameter τ_5 (0 = square pyramidal; 1 = trigonal bipyramidal).[65] [c] Only those within equatorial plane. [d] Only two trans angles (within square plane). [e] Only one trans angle (axial to trigonal plane).

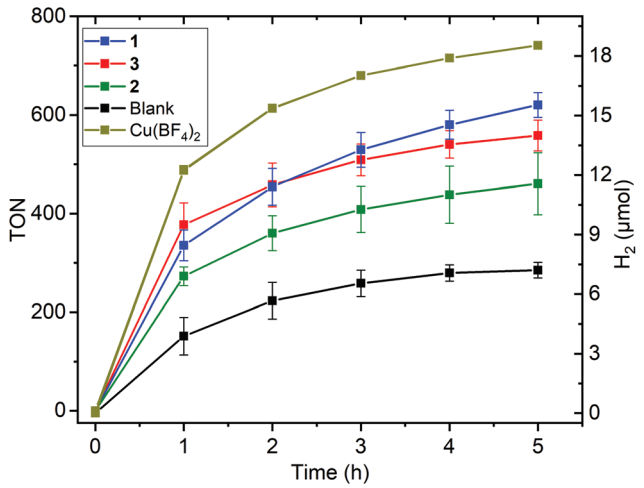

Fig. 5 Hydrogen evolution (TON left, μmol right; see Fig. S12† for this plot in terms of hydrogen volume in mL) *vs.* time profile for copper complexes **1** $[Cu^{II}L^{Et}]BF_4$ (blue), **2** $[Cu^{II}L^{Et\text{-}MePy}]BF_4$ (green), and **3** $[Cu^{II}L^{EtPy2}]BF_4$ (red), as well as for the blank run with no copper catalyst (black) and the control experiment using the simple $Cu(BF_4)_2$ salt as the copper catalyst (olive), in DMF (C_{cat} = 5 μM) on irradiation with a blue LED (λ = 445 nm, 88 mW cm^{-2}) at 20 °C, with 1.0 M TEOA, 0.2 mM $[Ru(bpy)_3](PF_6)_2$ and 0.1 M HBF_4/0.53 M H_2O. Error bars show the standard deviation from the mean, calculated in Origin from multiple separate runs (Tables 2, S1 and Fig. S14–S17†).

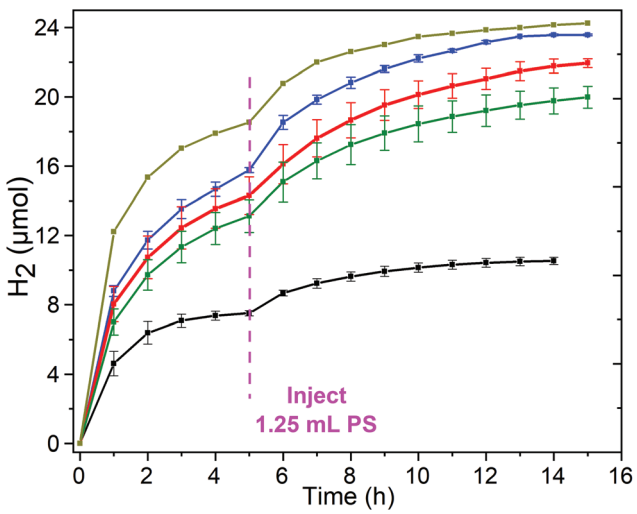

Fig. 6 Hydrogen evolution-time profile for copper complexes **1–3** in DMF (C_{cat} = 5 μM), with a fresh 1.25 mL aliquot of PS solution (0.2 mM) added after 5 h, (blue) **1** $[Cu^{II}L^{Et}]BF_4$, (red) **3** $[Cu^{II}L^{EtPy2}]BF_4$ and (green) **2** $[Cu^{II}L^{Et\text{-}MePy}]BF_4$ as well as for the 'blank' run with 0.2 mM $[Ru(bpy)_3](PF_6)_2$ (black) and the control experiment of $Cu(BF_4)_2$ salt (dark yellow). Conditions: Irradiation with a blue LED (λ = 445 nm, 88 mW cm^{-2}) at 20 °C, with 1.0 M TEOA, 0.2 mM $[Ru(bpy)_3](PF_6)_2$ and 0.1 M HBF_4/0.53 M H_2O. Error bars show the standard deviation from the mean, calculated from two separate runs (Table 3 and Fig. S18–S21†).

and 5.7 μmol of hydrogen, respectively. These results are consistent with the deactivation of the system being caused in part by the decomposition of the PS,[67] but also in part by decomposition of the catalyst and/or the sacrificial donor. Partial restoration of activity on addition of a second aliquot of $[Ru(bpy)_3]^{2+}$ has previously been reported for other photocatalytic HER systems: (a) a heptacoordinated Co^{II} catalyst in aqueous media where 40% of the activity was restored,[68,69] and (b) a Co^{II} metallopeptide catalyst in neutral water where just 6% of activity was restored, and where they also noted that blue irradiation led to faster loss of activity than green light did.[70]

Clearly the fairly short time over which high photocatalytic HER activity is observed for these three copper complexes is a key limitation for the present system, so whilst these complexes double the number of molecular copper catalysts known

Table 2 Performance of copper complexes **1–3**, as well as that of the blank and control, in blue-light-driven HER in DMF solution. Conditions: 6 h irradiation with a blue LED (λ = 445 nm, 88 mW cm^{-2}) at 20 °C, 5 μM catalyst, 1 M TEOA sacrificial reductant, 0.2 mM $[Ru(bpy)_3](PF_6)_2$ PS, 0.1 M HBF_4/0.53 M H_2O. For more details see the ESI†

Catalyst	TON (mol_{H_2} mol_{cat}^{-1})	H_2 (μmol)	TOF_{max} (min^{-1})
1	620 ± 20	15.5 ± 0.6	16 ± 1
2	460 ± 60	11.4 ± 1.7	12 ± 3
3·0.5H_2O	560 ± 30	14.0 ± 0.7	16 ± 2
$Cu(BF_4)_2{\cdot}xH_2O$[a,b]	740	18.5	26
$Cu(NO_3)_2{\cdot}3H_2O$[a,b]	720 ± 20	17.9 ± 0.4	24 ± 3
No copper[a,c]	290 ± 10[e]	7.2 ± 0.4	5 ± 1[e]
Dark[a,d]	0	0	0

[a] Blanks run under the same conditions except: [b] cat = simple salt or [c] no cat or [d] no light. [e] Calculated assuming 5 μM catalyst was present (it's not) which enables comparison with the other TONs. NB. TON = 290 is TON_{PS} = 7.

Table 3 Evolution of hydrogen by copper complexes (**1–3**, blank and $Cu(BF_4)_2$), before and after the addition of a fresh aliquot of PS solution (same aliquot as initially added)

Complex	H_2/μmol first cycle[a]	H_2/μmol second cycle[b]	Restored activity[c] (%)
1	15.8	7.8	49
2	13.1	6.7	51
3·0.5H_2O	14.3	7.6	53
No copper	7.5	2.5	33
$Cu(BF_4)_2$	18.5	5.7	31

[a] 5 h irradiation with a blue LED (λ = 445 nm, 88 mW cm^{-2}) at 20 °C, sacrificial reductant = 1 M TEOA, PS = 0.2 mM $[Ru(bpy)_3](PF_6)_2$, proton source = 0.1 M HBF_4/0.53 M H_2O and 5 μM catalyst. [b] Reaction vessel was injected by 1.25 mL PS (same aliquot as used initially) after blue LED light irradiation for 10 hours. [c] Restored activity = H_2 produced during the second cycle × (100)/H_2 produced during the first cycle.

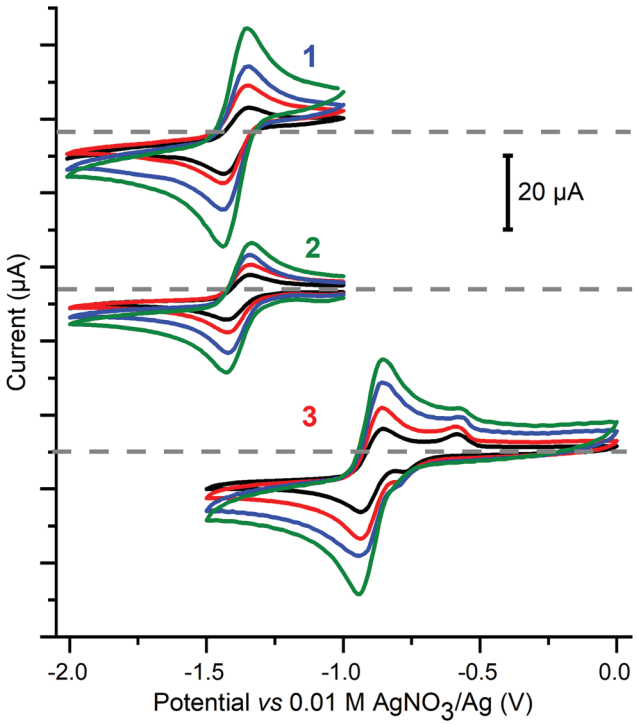

Fig. 7 Cyclic voltammetry of the reversible redox processes seen at negative potentials for 1 mM MeCN solutions of **1** (top, $E_{1/2}$ = −1.39 V, ΔE = 0.09 V, D = 7.7 × 10^{-6} cm^2 s^{-1}), **2** (middle, $E_{1/2}$ = −1.39 V, ΔE = 0.09 V, D = 3.4 × 10^{-6} cm^2 s^{-1}), and **3** (bottom, $E_{1/2}$ = −0.89 V, ΔE = 0.09 V, D = 5.4 × 10^{-6} cm^2 s^{-1}) Conditions: 0.1 M $(Bu_4N)PF_6$, glassy carbon working electrode (d = 3 mm, A = 0.071 cm^2), 293 K, *vs.* 0.01 M $AgNO_3$/Ag. In this system $E_{1/2}(Fc^+/Fc)$ = 0.09 ± 0.01 V, with ΔE = 0.09 V, and this was unchanged even after 6 h of electrolysis (Fig. S31†). Scan direction: for **1** and **2** −1.0→−2.0→−1.0 V, for **3** 0.0→−1.5→0.0 V; scan rate: 50 (black), 100 (red), 200 (blue) and 400 (green) mV s^{-1}; grey dashed lines correspond to zero current for each set of CVs.

to be active in photocatalytic HER (Fig. 1, box), the finding that the control is an even more active catalyst puts this into stark perspective. Hence our attention instead turned to the potential of **1–3** as electrocatalysts for HER.

Electrocatalytic hydrogen evolution

First the cyclic voltammetry data were obtained for **1–3** as well as for the control, $Cu(BF_4)_2{\cdot}xH_2O$, at 1 mM of copper(II) in dry MeCN with 0.1 M Bu_4NPF_6 *vs.* 0.01 M $AgNO_3$/Ag using a glassy carbon working electrode (Fig. 7 and S22†).

All three copper complexes, **1–3**, show a reversible redox process, at −1.39 V for square planar **1**, −1.39 V for square pyramidal **2**, and −0.89 V for trigonal bipyramidal **3** (Fig. 7), whereas the control experiment shows an irreversible process at approximately E_{pc} = −1.0 V (Fig. S23†), all *versus* a 0.01 M $AgNO_3$/Ag reference electrode. It is interesting to note that the pair of macrocyclic complexes (**1** and **2**), in which a square plane of donors is enforced upon the copper centre, have identical $E_{1/2}(Cu^+/Cu^{2+})$ values (−1.39 V), whereas the non-cyclic ligand complex (**3**) allows the copper centre to adopt a trigonal bipyramidal geometry, and this complex is far easier to reduce ($E_{1/2}(Cu^+/Cu^{2+})$ = −0.89 V) than the other two complexes. It is also important to note that (before adding acid) there is no evidence of a stripping wave in the CVs of **1–3** (Fig. S22, ESI†).

The linear current *vs.* square root of scan rate plots for **1** to **3** (Fig. S24†) confirm that these $Cu^{2+} \leftrightarrow Cu^+$ redox events are reversible and diffusion controlled. Furthermore, this enables the use of the Randles–Sevcik equation[71,72] to determine the diffusion coefficients (D, cm^2 s^{-1}) for each complex: 7.7 × 10^{-6} for **1**, 3.4 × 10^{-6} for **2**, and 5.4 × 10^{-6} for **3** (see the ESI† for more details). This is in the same ballpark as the diffusion coefficient of 1.24 × 10^{-5} cm^2 s^{-1}, determined in aqueous phosphate buffer (pH = 12), for a copper(II) complex of a tetradentate N_4-donor ligand with a dangling OH head unit, used as a catalyst for the water oxidation reaction (WOR).[73]

Next, each of the three complexes **1–3**, and $Cu(BF_4)_2{\cdot}xH_2O$ as a control, were tested as HER electrocatalysts in the presence of acetic acid (Fig. 8–11 and S25†). Acetic acid was chosen as the acid source as in MeCN it has two key advantages, low homoconjugation,[74,75] and being a weak acid (pK_a = 23.5)[76,77] which results in long catalyst lifetimes – but a key disadvantage is that it is challenging to reduce the protons to

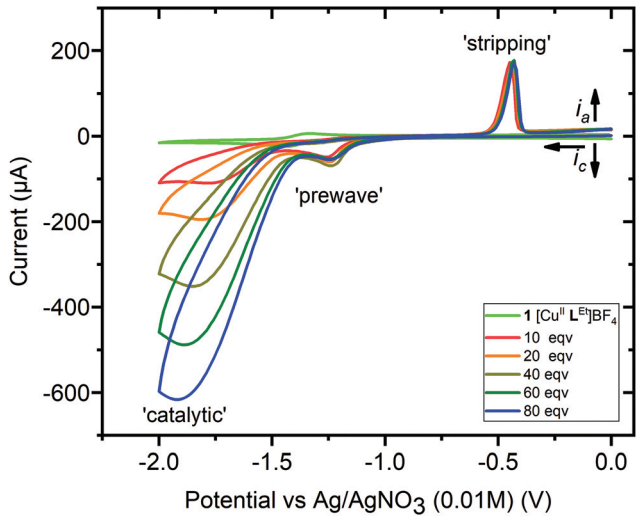

Fig. 8 Cyclic voltammetry, 0→−2.0→0 V *vs.* 0.01 M $AgNO_3$/Ag, for a 1 mM MeCN solution of **1** (light green, no acid), with successive additions of 10 or 20 equivalents of acetic acid (see key), up to a total of 80 equivalents (blue) = 80 mM, with increasing [acid] leading to increasing catalytic wave currents. Conditions: 0.1 M $(NBu_4)PF_6$, glassy carbon working electrode (d = 3 mm, A = 0.071 cm^2), 293 K, scan rate 100 mV s^{-1}. Before and after this study, $E_{1/2}(Fc^+/Fc)$ = 0.09 ± 0.01 V, with ΔE = 0.09 ± 0.01 V (see Fig. S25†).

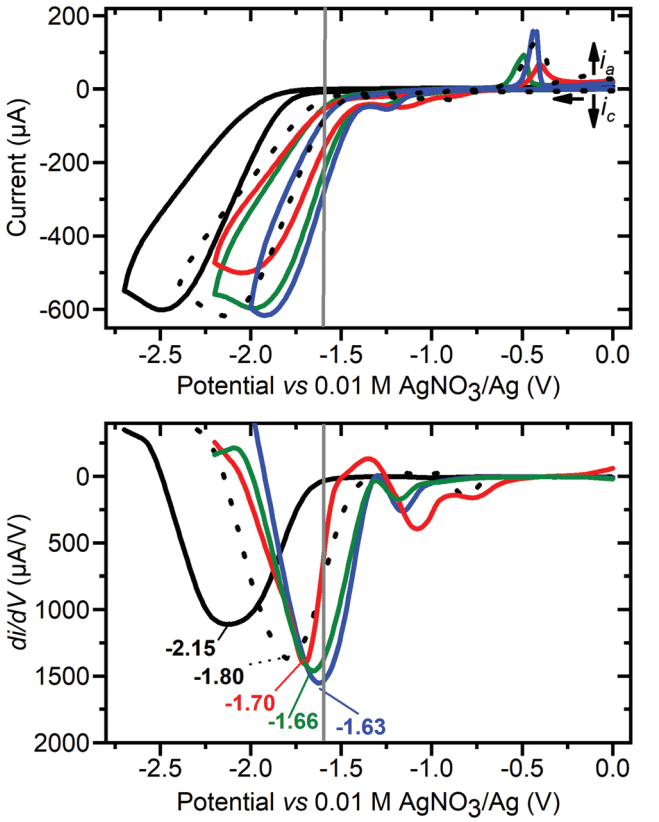

Fig. 9 (Top) Cyclic voltammograms of 80 mM acetic acid in MeCN (control, black line) in the presence of 1 mM: $Cu^{II}(BF_4)_2{\cdot}xH_2O$ (black dots), **2** (green), **3** (red) and **1** (blue). (Bottom) The first derivative of the forward scan of each CV, annotated with E_{inf} (potential at inflection point in V *vs.* 0.01 M $AgNO_3$/Ag), 80 mM acetic acid (−2.15, black line), in the presence of 1 mM: $Cu^{II}(BF_4)_2{\cdot}xH_2O$ (−1.80, black dots), **3** (−1.70, red), **2** (−1.66, green) and **1** (−1.63, blue). Conditions: 100 mV s^{-1}, 0.1 M $(Bu_4N)PF_6$, glassy carbon working electrode (d = 3 mm, A = 0.071 cm^2), 293 K. The grey vertical line at −1.6 V is the $E_{applied}$ used in the controlled potential coulometry studies. Before and after each of these studies, $E_{1/2}(Fc^+/Fc)$ = 0.09 ± 0.01 V, with ΔE = 0.09 ± 0.01 V (see Fig. S25†).

form H_2, due to a relatively high thermodynamic potential ($E^\circ_{H^+/H_2} = -1.42$ V *vs.* Fc^+/Fc on glassy carbon in 0.1 M Bu_4NPF_6 in MeCN, which is approx. −1.41 V *vs.* 0.01 M $AgNO_3$/Ag).[74,77]

The CVs of each of the complexes, **1**–**3**, were then obtained in the presence of increasing concentrations of acetic acid, and these showed catalytic waves, with the maximum current increasing with acid concentration (Fig. 8 and S25†). For complexes **1** and **2** a small prewave is observed (Fig. S32; Table S4†), at a more positive E_p value (−1.24 to −1.33 V) than the reversible process seen when no acid is present (−1.42 to −1.43 V), whilst for complex **3** the reversible process seen when no acid is present (−0.93 V) continues to be observed, and at a more positive E_p value than the prewave that is also seen after adding acid (−1.17 to −1.29 V).

In addition, whilst there is no evidence of a stripping wave in the CVs of these three complexes before adding acid (light green trace in Fig. 8; also Fig. S33, ESI†), after adding acetic acid a small stripping wave, consistent with the deposition of some Cu^0 on the working electrode,[35,36] is seen for all three complexes, **1**–**3**, between −0.44 and −0.50 V (Fig. 8 and S25†). The results in the case of the simple salt are very different: the stripping peak is present before adding any acid, at −0.53 V, and this shifts to −0.33 V as acid is added (Fig. S25†).

Next the blank (Fig. 9, black, no added copper compound) for 80 mM acetic acid was run at 100 mV s^{-1}, giving E_{pc} = −2.45 V and E_{inf} = −2.15 V *vs.* 0.01 M $AgNO_3$/Ag (where E_{inf} is the irreversible reduction potential inflection point[74]). These are similar to those reported by Dempsey and co-workers under similar conditions but with 25 mM acetic acid (E_{inf} = −2.38 V *vs.* Fc^+/Fc, which is approx. −2.30 V *vs.* 0.01 $AgNO_3$/Ag).[74] Then the various copper complexes were added to the 80 mM acetic acid: **1** resulted in the smallest E_{pc} for proton reduction (E_{pc} = −1.91 V, E_{inf} = −1.63 V, and the potential corresponding to half the maximum catalytic current $E_{cat/2}$ = −1.60 V) with the onset potential of the catalytic wave at about −1.37 V, followed by **2** (E_{pc} = −2.01, E_{inf} = −1.66 and $E_{cat/2}$ = −1.66 V), **3** (E_{pc} = −2.04, E_{inf} = −1.70 and $E_{cat/2}$ = −1.66 V) and then $Cu(BF_4)_2{\cdot}xH_2O$ (E_{pc} = −2.16, E_{inf} = −1.80 and $E_{cat/2}$ = −1.78 V).

The promising electrocatalytic HER activity seen in the case of **1** is also indicated by an i_{cat}/i_p ratio of 34 at 100 mV s^{-1} with [cat] = 1 mM, [acetic acid] = 80 mM, and 20 °C, where i_{cat} is peak catalytic current and i_p is peak current in absence of acid. This is comparable to that reported for copper catalyst **G** (i_{cat}/i_{pc} = 24),[51] and also to DuBois's nickel catalyst (i_{cat}/i_{pc} = 38 and 74 in dry and wet MeCN, respectively).[78] A much higher i_{cat}/i_p

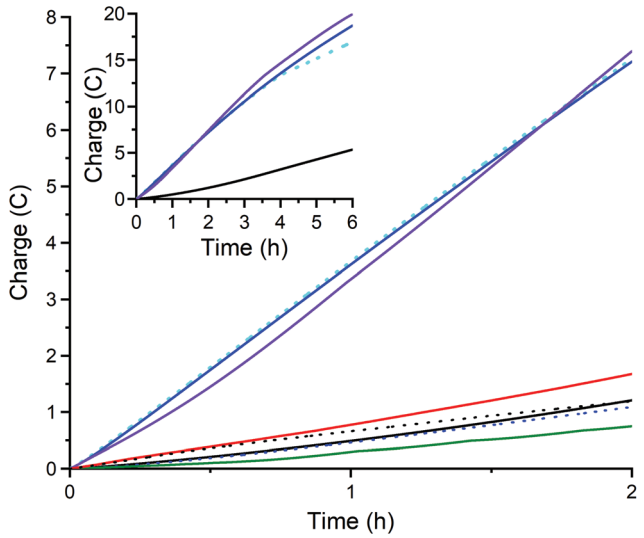

Fig. 10 Charge transferred during controlled potential electrolysis at −1.60 V of an 8 mL solution of 80 mM acetic acid (black line, blank) in the presence of 1 mM: **1** (duplicate runs, blue and violet), **2** (green), **3** (red), $Cu^{II}(BF_4)_2{\cdot}6H_2O$ (black dots, control). After electrolysis with **1** the glassy carbon working electrode (d = 3 mm, A = 0.071 cm^2) was gently rinsed with acetonitrile and the electrolysis repeated in freshly made electrolyte with 80 mM acetic acid but without adding catalyst (blue dashes; rinse and repeat test; confirms there is no catalytically active deposit on the working electrode). Tests on **1** in the absence of mercury (duplicate runs, blue and violet) and in the presence of 1 mL of mercury drop (sky blue dots) confirm the absence of catalytically active nanoparticles. The inset shows extended electrolysis of 6 hours, carried out for the blank run and for the three runs of complex **1** (with and without mercury drop). Also see Table S3.†

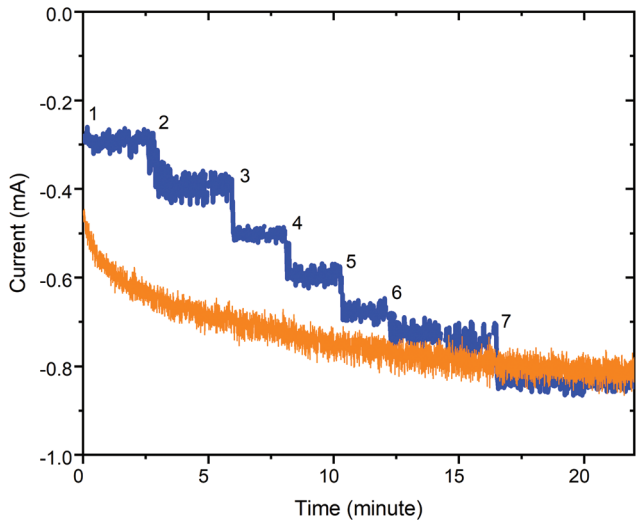

Fig. 11 Plot of current response *versus* time at E = −1.6 V *vs.* $Ag/AgNO_3$ (0.01 M) for a 0.33 M acetonitrile solution of **1** when the acetic acid is either (blue) added in 7 portions reaching 80 mM in H^+ after the 7th addition or (orange) it is 80 mM from the start. Conditions: Glassy carbon working electrode (d = 3 mm, A = 0.071 cm^2), 20 °C, and Pt counter electrode. Also see Table S3.†

of 303 was reported for copper corrole **D1** using TFA (160 mM) and water (2.4 M) in acetonitrile.[44]

To further evaluate the catalytic activity of **1** for hydrogen evolution, controlled potential coulometry (see Fig. S26 for the electrochemical cell and Table S3† for key data) was carried out at $E_{applied}$ = −1.60 V for 2 hours (Fig. 9 and 10), using a small glassy carbon working electrode (diameter 3 mm, A = 0.071 cm^2). As shown in Fig. 10, complexes **2** (green) and **3** (red) – as well as the control, $Cu^{II}(BF_4)_2{\cdot}xH_2O$ (black dots) and the blank (black line) – all showed minimal activity (<1.7C, 2.2e per metal center, TON < 1.1) whereas complex **1** (blue and violet) stood out, transferring an average charge of 7.3C over 2 hours (9.5e per **1**, TON = 4.7) with bubbles seen forming underneath the electrode (Fig. S26†).

The 'overpotential necessary for catalysis'[74,79] ($E_{cat/2}$ = −1.64 V) minus $\left(E^{\circ}_{H^+/H_2} = -1.41\,V\right)$ of about 0.23 V for complex **1** is at the low end of related values reported for the handful of molecular copper(II) HER electrocatalysts in the literature to date (Fig. 1): 'onset overpotentials' for **A** (0.420 V) in aqueous phosphate buffer solution (pH 2.5),[42] for **G** (0.440 V) for acetic acid in DMF/H_2O (95 : 5 v/v);[51] 'overpotentials' for **D** (0.450 V) for trifluoroacetic acid (TFA) in acetonitrile (determined using $E_{cat/2}$),[44] and in water at pH = 7 for **B2** (0.636 V),[46] **C3** (0.639 V)[47] and **B1** (0.817 V).[45] But, as noted by Dempsey, such overpotentials "should not be considered a general parameter for direct, quantitative, catalyst comparison between independent reports because of the nonuniform use of the parameter E_{cat}".[80]

Given ongoing activity shown by **1** over the first 2 hours of controlled potential electrolysis at −1.6 V, this was continued for a total of 6 hours, resulting in an average total of 19.3C being transferred – with the catalyst retaining an almost constant level of activity throughout the 6 hours period (Fig. 10, inset, duplicate runs in blue and violet). *i.e.* after 2 hours 7.3C is transferred, so 3 times this gives an expected transfer of 21.9C after 6 hours, which is close to the 19.3C observed, consistent with **1** having a relatively long lifetime as an HER electrocatalyst. The 19.3C transferred equates to 25.0e per **1**, so to a TON(H_2) of 12.5 (assuming 100% FE). Clearly this TON could be further increased by use of a larger surface area electrode and/or running the electrolysis for longer as the catalyst clearly remains active after 6 hours. Nevertheless, the present TON (H_2) of 12.5 compares favorably to the TON(H_2) of 11 reported for DuBois's 0.90 M nickel catalyst in acetonitrile, using 0.43 M [(DMF)H]OTf, (OTf = triflate or trifluoromethanesulfonate) and 1.2 M of water, over 30 minutes, after which the catalyst has decomposed,[78] and the TON of 23 for 0.30 M copper corrole **D** (Fig. 1) in acetonitrile, with TFA (180 mM), over 2 hours.[44]

Notably, further controlled potential electrolysis test runs at −1.6 V, with a third of the catalyst concentration (0.33 mM in **1**), show that **1** remains an effective electrocatalyst for HER at this lower catalyst loading, regardless of whether the 80 mM acetic acid is present from the start (Fig. 11, orange trace), or is added in 7 aliquots (Fig. 11, blue trace). Immediate current growth is seen (steps) each time an aliquot of acetic acid is

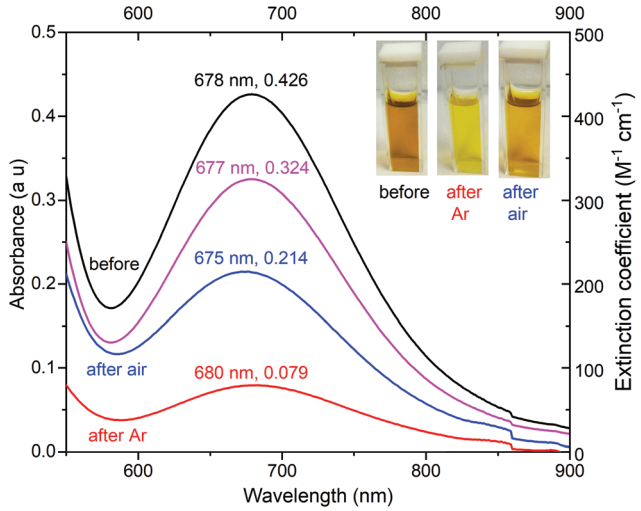

Fig. 12 UV-vis spectra, focusing on the d–d band, of 1 mM $[Cu^{II}L^{Et}]BF_4$ (**1**), in the presence of 80 mM acetic acid in 0.1 M Bu_4NPF_6/MeCN: (black) before electrolysis commenced, (red) immediately after 6 hours electrolysis, (blue) after the post-electrolysis solution was exposed to air for 30 minutes, and (pink) is the blue curve recalculated in 10.5 not 8 mL (allowing for diffusion into the central compartment). Electrolysis conditions: Glassy carbon working electrode (d = 3 mm, A = 0.071 cm^2), 20 °C, and Pt counter electrode. For the full range UV-vis spectra see Fig. S29.†

added (blue trace), and the overall result after 23 minutes is that it has approximately the same current flow $i_{25\ min}$ = −0.85 mA (transferred a total of 0.82C; 3.2e^- per **1**) as that obtained after 23 minutes when it is 80 mM in acid from the start $i_{25\ min}$ = −0.81 mA (total of 1.00C; 3.9e^- per **1**).

Given these promising findings, further checks were made on complex **1**. Firstly, it was shown to be stable in 90 mM acetic acid for at least 5 hours, by monitoring the UV-vis spectrum (Fig. S28†). Secondly, before electrolysis the solution of **1** is dark golden yellow whereas during electrolysis it turns bright yellow (Fig. 12). After electrolysis, on exposure to air for 30 min (electrodes removed) it darkens again to gold yellow, albeit not returning fully to the original colour (Fig. 12 and S29†), even after longer air exposure. In part this is due to some diffusion of the catalyst into the central compartment of the "H" cell (Fig. S26†) during the 6 hours of electrolysis, reducing the concentration of the solution in the working electrode chamber: the pink trace in Fig. 12 shows an estimated correction to the UV-Vis spectrum (after exposure to air for 30 min) for this dilution, and is consistent with 76% of **1** being intact at this point.

Thirdly, the reference electrode was checked against Fc^+/Fc before and after the 6 h electrolysis and was unshifted (Fig. S31†).

Fourthly, a rinse and repeat experiment – whereby the electrode was removed after 6 hours of controlled potential electrolysis at −1.60 V, gently rinsed with MeCN, and then placed into a fresh solution for electrolysis (without adding catalyst) showed minimal activity over the next 2 hours (blue dashed lines in Fig. 10), indicating that no catalytically active heterogeneous deposit was present on the electrode surface. Nevertheless, future studies will probe this point further, as this may well prove to be a case of a false negative (see introduction). Another key test performed was the mercury drop test: the 6 h electrolysis of **1** was repeated in same manner as before except that 1 mL of mercury was added (Fig. 10, sky blue dots). Pleasingly, a similar amount of charge (17.0C after 6 h; 7.2C after 2 h) was passed as when no mercury was present (average 19.3C after 6 h; 7.3 after 2 h; blue and violet), which indicates that the electrocatalytic activity is probably not due to nanoparticles or similar having formed. Whilst the results of both of these additional tests[42,43] are consistent with the catalytically active species being homogeneous, not heterogeneous (see Fig. S29 and S30 in the ESI† for more details), future studies will probe this point further, as a small stripping wave is seen, and false negatives are not uncommon.

Conclusions

Inspired by the promising HER activity, under photocatalytic conditions, seen for (a) just three copper complexes to date[24,48,51] and (b) the cobalt complex of the N_4-donor [1 + 1] Schiff base macrocycle HL^{Et} (made by the condensation of diphenylamine-2,2′-dicarboxaldehyde and diethylenetriamine) reported by some of us,[16] herein the number of such copper catalysts is doubled.

Firstly, two new N_5-donor diphenylamine-based ligands have been prepared and characterised: an 'armed' macrocycle $HL^{Et\text{-}MePy}$ formed by alkylation of HL^{Et}, and a non-cyclic analogue HL^{EtPy2}. Secondly, 1 : 1 reactions of the respective ligand with copper(II) tetrafluoroborate in the presence of TEA, gave the literature complex $[Cu^{II}L^{Et}]BF_4$ (**1**)[59] and the two new complexes $[Cu^{II}(L^{Et\text{-}MePy})]BF_4{\cdot}0.5H_2O$ (**2**·0.5H_2O) and $[Cu^{II}(L^{EtPy2})]BF_4$ (**3**). Single crystal structure determinations reveal contrasting copper(II) geometries: square planar in **1**, square pyramidal in **2** and trigonal bipyramidal in **3**.

Interestingly, despite the contrasting copper(II) geometries, all three of these readily prepared complexes, **1–3**, have similar HER activities (TON 460–620) under the photocatalytic conditions employed (sacrificial reductant TEOA, PS $[Ru(bpy)_3]^{2+}$, proton source HBF_4, irradiated by blue LED). But, disappointingly, on running the appropriate control and blank tests – not reported for the previous copper HER catalysts in the literature – complexes **1–3** are revealed to be no more active than the simple salts copper(II) tetrafluoroborate/nitrate (TON 720–740). This study therefore highlights the importance of always doing, and reporting, the results of blanks and controls, in order to put the observed activity of the complexes studied into proper context.

In all cases (copper complexes/salts), partial activity is restored on adding a second aliquot of PS after 5 hours, consistent with the drop in activity being due in part to PS decomposition, along with decomposition of the complex and sacrificial electron donor. This, taken with the fact that the blank run with no copper catalyst present shows about half the

HER activity of complexes **1–3**, indicates that a more stable PS (*e.g.* Ir–PS[48]), and/or irradiation wavelength (*e.g.* green not blue[70]), should be used in future tests.

But, given the disappointing photocatalytic HER results for **1–3**, our attention instead turned to testing them for electrocatalytic HER. Pleasingly all three complexes, **1–3**, show reversible redox processes at −0.89 (trigonal bipyramidal **3**) and −1.39 (square planar **1** and square pyramidal **2**) V *vs.* 0.01 M $Ag/AgNO_3$. Furthermore, the square planar macrocyclic complex **1** shows *good and ongoing electrocatalytic HER activity* at −1.60 V for 6 h, with a $TON(H_2)_{6\ h} = 12.5$, whereas both of the other complexes (**2** and **3**), and the control, showed similar, much more modest activity, with $TON(H_2) < 1.1$ compared with 4.7 for **1**, after 2 hours.

Hence the key finding of this study is that square planar copper complex **1** is, or forms, a *promising and robust electrocatalyst* for HER, showing (a) good and robust ongoing activity even after 6 hours, and (b) mercury drop, as well as 'rinse and repeat', test results that are consistent with homogeneous, not heterogeneous, electrocatalysis occurring. *But* false negatives for such tests can occur, and small stripping waves are seen, so the nature of the catalytically active species will be probed further in future studies. Given the identical redox potentials in MeCN (−1.39 V *vs.* 0.01 M $Ag/AgNO_3$) for the pair of macrocyclic complexes, square planar **1** (NH in ligand backbone) and the closely related but square pyramidal **2** (no NH in ligand backbone), the difference in electrocatalytic HER activity is interesting and should also be probed further in the future. The importance of proton relays, facilitated by NH moieties, has been demonstrated by others,[81–85] and may also be the key here. But if the electrocatalytically active species proves to be heterogeneous, then clearly the nature of that species is dependent on the choice of precursor.

In the longer term we aim to improve the activity and lifetime of these catalysts (a) for photocatalytic HER by further refining the 'mix' of components and the irradiation wavelength used, and (b) for electrocatalytic HER by employing other 3d metal ions and modifying the ligand skeleton further to develop new members of this promising new family, in particular aiming for new members that retain NH functionality. But our immediate priorities are more in depth electrocatalytic testing of the promising electrocatalyst **1**. First we will carry out additional tests to identify whether or not a metastable heterogeneous deposit, not seen in the rinse and repeat test, is being formed, and if so what it is composed of. Other tests will include longer runs, runs with added water and in aqueous solution, probing the kinetics, and getting a local gc set up to quantify (H_2), as well as testing these copper catalysts for activity in the photo- and electro-catalytic CO_2 reduction reaction (CO_2RR).

Experimental section

Elemental analyses (C, H, N) were determined at the Campbell Microanalytical Laboratory, University of Otago. ^{1}H and ^{13}C NMR spectra were recorded on a Varian 400 or 500 MHz NMR spectrometer at 298 K. Chemical shifts are reported in parts per million and referenced to the residual protonated solvent peak in the ^{1}H NMR spectra and the residual solvent peak in the ^{13}C NMR spectra [$CDCl_3$: 7.26 ppm (^{1}H) and 72.16 ppm (^{13}C); d_6-DMSO: 2.50 ppm (^{1}H) and 39.52 ppm (^{13}C)]. ESI MS spectra (Fig. S42–S45†) were collected on a Bruker MicrOTOF$_Q$ spectrometer. UV-vis spectra were obtained on a Varian 500 Scan UV-vis-NIR spectrophotometer. Infrared (IR) spectra were recorded on a Bruker ATR-IR spectrometer with a diamond anvil Alpha-P module, within the range of 400–4000 cm^{-1}. Crystallographic data for the structures have been deposited with the Cambridge Crystallographic Data Centre, CCDC 1983967–1983968.† Photo- and electro-catalysis testing instrumentation and details are provided in the ESI.†

General synthetic procedures

Methanol and acetonitrile were HPLC grade and other solvents were reagent grade. TEA (Fisher Scientific), 2-(bromomethyl) pyridine hydrobromide (AKSci) and 2-aminoethylpyridine (Aldrich) were bought and used as supplied. Diethylene triamine (Fisher) was purified by distillation under a reduced pressure of 200 mbar and temperature of 100 °C. **Dpa** and HL^{Et} were prepared by the literature procedures.[59,86] All reactions were carried out by AA (Otago) and were conducted in air unless otherwise stated.

$HL^{Et\text{-}MePy}$·0.5CH_2Cl_2. This '*N*-(2-methylpyridyl)-armed' macrocycle was prepared under nitrogen by adding TEA (0.61 g, 0.84 mL, 6.16 mmol) to a yellow dry THF solution (60 mL) of the macrocycle HL^{Et} (0.60 g, 2.0 mmol). The mixture was stirred at room temperature for 10 minutes, then 2-(bromomethyl)pyridine hydrobromide (0.54 g, 2.12 mmol) was then added and the resulting solution was stirred at room temperature for 2 days, over which time the colour gradually changed from yellow to bright red to turbid yellow. Then it was filtered (to remove TEA·HBr) and filtrate was taken to dryness under reduced pressure to give a red oily residue which was dissolved in CH_2Cl_2 (60 mL) and washed with saturated aq. $NaHCO_3$ (2 × 40 mL). The organic layer was dried over anhydrous $MgSO_4$, filtered and then taken to dryness under reduced pressure to give a red oil, which after drying overnight *in vacuo* yielded $HL^{Et\text{-}MePy}$·0.5CH_2Cl_2 as a red solid (0.51 g, yield: 63%). Microanalysis calcd for $C_{24}H_{25}N_5$·0.5CH_2Cl_2 (%): C, 69.08; H, 6.15; N, 16.44. Found C, 69.45; H, 6.23; N, 16.26. λ_{max}/nm (MeCN) (ε/dm^3 mol^{-1} cm^{-1}) = 360 (2825). ^{1}H NMR (400 MHz, DMSO-d_6) δ (ppm) = 12.35 (s, 1H, NH), 8.48 (s, 2H, $H_{7,\ 7'}$), 8.36–8.30 (m, 1H, H_{11}) 7.57 (dd, J = 8.4, 1.1 Hz, 2H, $H_{6,\ 6'}$), 7.52 (dd, J = 7.7, 1.7 Hz, 2H, $H_{3,\ 3'}$), 7.35 (ddd, J = 8.5, 7.2, 1.7 Hz, 2H, $H_{5,\ 5'}$), 7.21 (dt, J = 7.1, 1.1 Hz, H_{13}), 7.05–6.97 (m, 2H, H_{12}, H_{14}), 6.94 (td, J = 7.4, 1.0 Hz, 2H, $H_{4,\ 4'}$), 3.75 (s, 2H, H_{10}), 3.65 (m, 4H, $H_{9,\ 9'}$), 2.81–2.68 (m, 4H, $H_{8,\ 8'}$). 5.8 (s, 1H DCM signal). ^{13}C NMR (400 MHz, DMSO-d_6, 298 K) δ (ppm) = 162.81 (C_7), 160.34 (C_{15}), 148.68 (C_{11}), 142.61 (C_1), 135.81 (C_{13}), 131.60 (C_3), 131.21 (C_5), 123.53 (C_2), 123.50 (C_{14}), 122.09 (C_{12}), 120.24 (C_4), 116.35 (C_6), 59.45 (C_{10}), 57.67 (C_9), 54.39 (C_8). ESI-MS m/z = 384.2203 (calcd for $[C_{24}H_{25}N_5 + H]^+$ 384.2210). IR (ATR) ν, cm^{-1}: 2933, 2831, 1627, 1583, 1516, 1444, 1310, 1157, 739, 633.

HL^{EtPy2}·0.25$(CH_3)_2CO$. This 'two-armed' acyclic ligand was prepared by taking a bright yellow refluxing MeCN (40 mL) solution of **dpa** (0.30 g, 1.33 mmol) and adding 2-aminoethylpyridine (0.34 g, 2.80 mmol, 2.1 eq.). The resulting solution was refluxed for 3 hours, then stirred at room temperature overnight, before being taken to dryness under reduced pressure. The resulting yellow oily product was taken up in acetone (5 mL), then taken back to dryness under reduced pressure to produce HL^{EtPy2}·0.25$(CH_3)_2CO$ as a red sticky oil which is stored under vacuum (0.56 mg, 97%). Microanalysis calcd for $C_{28}H_{27}N_5$·0.25$CO(CH_3)$ (%): C, 77.07; H, 6.41; N, 15.63. Found C, 76.69; H, 6.60; N, 15.14. ESI-MS m/z = 456.2117 (calcd for $[C_{28}H_{27}N_5Na]^+$ 456.2159. ^{1}H NMR (400 MHz, DMSO-d_6) δ (ppm) = 11.33 (s, 1H, NH), 8.39 (dt, J = 4.3, 1.2 Hz, 4H, $H_{7,\,7'}$ and $H_{14,\,14'}$), 7.57 (dd, J = 7.7, 1.6 Hz, 2H, $H_{11,\,11'}$), 7.52 (td, J = 7.6, 1.9 Hz, 2H, $H_{4,\,4'}$), 7.28 (ddd, J = 8.6, 7.1, 1.6 Hz, 2H, $H_{13,\,13'}$), 7.20–7.15 (m, 4H, $H_{3,\,3'}$ and $H_{2,2'}$), 7.09 (ddd, J = 7.6, 4.8, 1.2 Hz, 2H, $H_{5,\,5'}$), 6.94 (td, J = 7.4, 1.1 Hz, 2H, $H_{12,\,12'}$), 3.91 (td, J = 7.2, 1.2 Hz, 4H, $H_{8,\,8'}$), 3.04 (t, J = 7.2 Hz, 4H, $H_{9,\,9'}$). 2.8 (s, 1H $(CH_3)_2CO$). ^{13}C NMR (400 MHz, d_6-DMSO, 298 K) δ (ppm) = 161.81 (C_{14}), 159.71(C_{10}), 149.34 (C_7), 143.04 (C_1), 136.51 (C_4), 131.68 (C_{11}), 131.38 (C_{13}), 123.87 (C_6), 123.60 (C_2), 121.68 (C_5), 120.74 (C_{12}), 117.99 (C_3), 60.80 (C_8), 39.61(C_9). ESI-MS m/z = 456.2117 (calcd for $[C_{28}H_{25}N_5Na]^+$ 456.2159. IR (ATR) (ν, cm^{-1}): 3313 (N–H), 3059 (=C–H), 2996 (C–H), 2911, 2843, 1630 (C=N), 1589, 1514, 1433, 1316, 1144, 1045, 984, 741, 605, 511.

$[Cu^{II}L^{Et}]BF_4$ (1). This complex was prepared by direct metalation of the pre-prepared HL^{Et} macrocycle (in the same way as previously reported for cobalt[59]) rather than metal template method reported previously for copper.[59] To a bright yellow solution of the macrocycle HL^{Et} (0.160 g, 0.54 mmol) dissolved in 25 mL of methanol/chloroform (1 : 1, v/v) was added TEA (0.070 mL, 0.54 mmol). The resulting bright yellow solution was stirred for 5 minutes at room temperature before $Cu^{II}(BF_4)_2$·H_2O (0.138 g, 0.54 mmol) was added, causing a sudden color change to deep red. The solution was stirred at 60 °C for 3 hours, then stirred at room temperature overnight. The resulting brown solid was collected by filtration and washed with diethyl ether (2 × 15 mL) and dried *in vacuo* to give **1** (0.21 g, 88%). Microanalysis calcd for $C_{18}H_{19}N_4BF_4Cu$ (%): C, 48.94; H, 4.34; N, 12.68. Found C, 48.88; H, 4.36; N, 12.70. ESI-MS m/z = 354.0902 (calcd for $[C_{18}H_{19}CuN_4]^+$ 354.0900). UV-Vis λ_{max}/nm (DMF) (ε/dm^3 mol^{-1} cm^{-1}) = 334 (4334), 401 (3762), 467 (13 500), 672 (453). Dark orange single crystals of **1** suitable for X-ray determination was grown by vapor diffusion of diethyl ether into a small sample of the reaction solution (1 mL).

$[Cu^{II}L^{Et\text{-}MePy}]BF_4$ (2). To a yellow solution of $HL^{Et\text{-}MePy}$ macrocycle (0.060 g, 0.156 mmol) and TEA (0.022 mL, 0.156 mmol) in 15 mL of methanol/chloroform (5 : 1, v/v) was added a blue methanol solution (2 mL) of $Cu^{II}(BF_4)_2$·H_2O (0.040 g, 0.156 mmol). The resulting deep red solution was stirred at 60 °C for 3 h, then stirred at room temperature overnight, before being vapor diffused with diethylether. Dark red needle-like crystals of **2**, suitable for a single crystal X-ray structure determination, formed over six days, and were collected by filtration, and washed with diethyl ether (2 × 15 mL) and dried *in vacuo* to give **2** (44 mg, 68%). Microanalysis calcd for $C_{24}H_{24}N_5BF_4Cu$ (%): C 54.10, H 4.54, N 13.14. Found C 53.81, H 5.00, N 12.83. ESI-MS m/z = 445.1293 (calcd for $[C_{24}H_{24}N_5Cu]^+$ 445.1322). UV-Vis λ_{max}/nm (DMF) (ε/dm^3 mol^{-1} cm^{-1}) = 336 (3793), 408 (3313), 479 (6216), 789 (342).

$[Cu^{II}L^{EtPy2}]BF_4$·0.5H_2O (3·0.5H_2O). To a yellow solution of HL^{EtPy2} ligand (0.060 g 0.140 mol) in MeCN/MeOH (1/1 v/v) (10 mL) was added TEA (0.020 mL, 0.140 mmol) and solution was stirred for 5 minutes before MeCN solution (1 mL) of $Cu^{II}(BF_4)_2$·H_2O (0.036 g, 0.140 mmol) was added, resulting in dark red solution. The solution was stirred at 60 °C for 3 h, then stirred at room temperature overnight, before being vapor diffused with diethylether. Dark red needle-like crystals of **3**, suitable for a single X-ray crystal structure determination, formed over 4 days, and were collected by filtration, and washed with diethyl ether (2 × 15 mL) and dried *in vacuo* to give **3**·0.5H_2O (50 mg, 72%). Microanalysis calcd for $C_{28}H_{26}N_5CuBF_4$·0.5H_2O (%): C 56.82, H 4.60, N 11.83. Found C 56.53, H 4.42, N 11.45. ESI-MS m/z = 495.1451 (calcd for $[C_{28}H_{26}N_5Cu]^+$ 495.1479). UV-Vis λ_{max}/nm (DMF) (ε/dm^3 mol^{-1} cm^{-1}) = 334 (5733), 403 (5371), 491 (10 128), 917 (309). IR (ATR) (ν, cm^{-1}): 3170, 3082, 1607, 1545, 1540, 1425, 1397, 1311, 1259, 1192, 1149, 1032, 879, 742, 633, 581, 513, 467.

Conflicts of interest

There are no conflicts to declare.

Acknowledgements

We thank the University of Otago for supporting this research (including a PhD scholarship AA) and the Catalyst Seed Fund (New Zealand) for supporting our collaborative studies (including exchange visits in both directions). GSH and OS also thank the Natural Sciences and Engineering Research Council (NSERC) of Canada for funding. Finally, we would like to thank the referees very much for taking the time to provide such detailed and constructive feedback, which has enabled us to significantly improve this manuscript.

Notes and references

1 J. F. Johnstone, C. D. Allen, J. F. Franklin, L. E. Frelich, B. J. Harvey, P. E. Higuera, M. C. Mack, R. K. Meentemeyer, M. R. Metz, G. L. Perry, T. Schoennagel and M. G. Turner, Changing disturbance regimes, ecological memory, and forest resilience, *Front. Ecol. Environ.*, 2016, **14**, 369–378.

2 T. P. Hughes, M. L. Barnes, D. R. Bellwood, J. E. Cinner, G. S. Cumming, J. B. C. Jackson, J. Kleypas, I. A. van de Leemput, J. M. Lough, T. H. Morrison, S. R. Palumbi,

E. H. van Nes and M. Scheffer, Coral reefs in the Anthropocene, *Nature*, 2017, **546**, 82.
3 A. L. Hammond, Solar energy: the largest resource, *Science*, 1972, **177**, 1088–1090.
4 N. Armaroli and V. Balzani, The Future of Energy Supply: Challenges and Opportunities, *Angew. Chem., Int. Ed.*, 2007, **46**, 52–66.
5 J. Su and L. Vayssieres, A Place in the Sun for Artificial Photosynthesis?, *ACS Energy Lett.*, 2016, **1**, 121–135.
6 S. Berardi, S. Drouet, L. Francas, C. Gimbert-Surinach, M. Guttentag, C. Richmond, T. Stoll and A. Llobet, Molecular artificial photosynthesis, *Chem. Soc. Rev.*, 2014, **43**, 7501–7519.
7 N. Armaroli and V. Balzani, The Hydrogen Issue, *ChemSusChem*, 2011, **4**, 21–36.
8 J. A. Turner, Sustainable hydrogen production, *Science*, 2004, **305**, 972–974.
9 Z. Han, F. Qiu, R. Eisenberg, P. L. Holland and T. D. Krauss, Robust photogeneration of H_2 in water using semiconductor nanocrystals and a nickel catalyst, *Science*, 2012, **338**, 1321–1324.
10 A. L. Goff, V. Artero, B. Jousselme, P. D. Tran, N. Guillet, R. Métayé, A. Fihri, S. Palacin and M. Fontecave, From Hydrogenases to Noble Metal–Free Catalytic Nanomaterials for H2 Production and Uptake, *Science*, 2009, **326**, 1384–1387.
11 C. V. Krishnan, B. S. Brunschwig, C. Creutz and N. Sutin, Homogeneous catalysis of the photoreduction of water. 6. Mediation by polypyridine complexes of ruthenium(II) and cobalt(II) in alkaline media, *J. Am. Chem. Soc.*, 1985, **107**, 2005–2015.
12 P. Du, J. Schneider, G. Luo, W. W. Brennessel and R. Eisenberg, Visible Light-Driven Hydrogen Production from Aqueous Protons Catalyzed by Molecular Cobaloxime Catalysts, *Inorg. Chem.*, 2009, **48**, 4952–4962.
13 A. Fihri, V. Artero, A. Pereira and M. Fontecave, Efficient H2-producing photocatalytic systems based on cyclometalated iridium- and tricarbonylrhenium-diimine photosensitizers and cobaloxime catalysts, *Dalton Trans.*, 2008, 5567–5569.
14 A. Fihri, V. Artero, M. Razavet, C. Baffert, W. Leibl and M. Fontecave, Cobaloxime-Based Photocatalytic Devices for Hydrogen Production, *Angew. Chem., Int. Ed.*, 2008, **47**, 564–567.
15 P. Zhang, M. Wang, C. Li, X. Li, J. Dong and L. Sun, Photochemical H2 production with noble-metal-free molecular devices comprising a porphyrin photosensitizer and a cobaloxime catalyst, *Chem. Commun.*, 2010, **46**, 8806–8808.
16 R. W. Hogue, O. Schott, G. S. Hanan and S. Brooker, A smorgasboard of 17 cobalt complexes active for photocatalytic hydrogen evolution, *Chem. – Eur. J.*, 2018, **24**, 9820–9832.
17 W. T. Eckenhoff, Molecular catalysts of Co, Ni, Fe, and Mo for hydrogen generation in artificial photosynthetic systems, *Coord. Chem. Rev.*, 2018, **373**, 295–316.
18 M. Nippe, R. S. Khnayzer, J. A. Panetier, D. Z. Zee, B. S. Olaiya, M. Head-Gordon, C. J. Chang, F. N. Castellano and J. R. Long, Catalytic proton reduction with transition metal complexes of the redox-active ligand bpy2PYMe, *Chem. Sci.*, 2013, **4**, 3934–3945.
19 Y. Huang and B. Zhang, Active Cocatalysts for Photocatalytic Hydrogen Evolution Derived from Nickel or Cobalt Amine Complexes, *Angew. Chem., Int. Ed.*, 2017, **56**, 14804–14806.
20 A. J. Esswein and D. G. Nocera, Hydrogen Production by Molecular Photocatalysis, *Chem. Rev.*, 2007, **107**, 4022–4047.
21 N. Queyriaux, R. T. Jane, J. Massin, V. Artero and M. Chavarot-Kerlidou, Recent developments in H_2 evolving molecular cobalt(II)–polypyridyl catalysts, *Coord. Chem. Rev.*, 2015, **304–305**, 3–19.
22 T. S. Teets and D. G. Nocera, Photocatalytic hydrogen production, *Chem. Commun.*, 2011, **47**, 9268–9274.
23 S. Losse, J. G. Vos and S. Rau, Catalytic hydrogen production at cobalt centres, *Coord. Chem. Rev.*, 2010, **254**, 2492–2504.
24 K. E. Dalle, J. Warnan, J. J. Leung, B. Reuillard, I. S. Karmel and E. Reisner, Electro- and solar-driven fuel synthesis with first row transition metal complexes, *Chem. Rev.*, 2019, 2752–2875.
25 J. A. Halfen, D. C. Fox, M. P. Mehn and L. Que Jr., Enhanced reactivity of copper catalysts for olefin aziridination by manipulation of ligand denticity, *Inorg. Chem.*, 2001, **40**, 5060–5061.
26 Y. Zhang, H.-C. Liang, L. N. Zakharov, S. K. Das, M. M. Hetu and A. L. Rheingold, Carboxyester hydrolysis promoted by Cu(II) complexes of pyridyl-amine carboxylate-pendant ligands, *Inorg. Chim. Acta*, 2007, 1691–1701.
27 L. Liang and D. Astruc, The copper(I)-catalyzed alkyne-azide cycloaddition (CUAAC) "click" reaction and its applications. An overview, *Coord. Chem. Rev.*, 2011, **255**, 2933–2945.
28 J. E. Hein and V. V. Fokin, Copper-catalyzed azide–alkyne cycloaddition (CuAAC) and beyond: new reactivity of copper (I) acetylides, *Chem. Soc. Rev.*, 2010, **39**, 1302–1315.
29 R. Angamuthu, P. Byers, M. Lutz, A. L. Spek and E. Bouwman, Electrocatalytic CO_2 Conversion to Oxalate by a Copper Complex, *Science*, 2010, **327**, 313–315.
30 Z. Chen and T. J. Meyer, Copper(II) Catalysis of Water Oxidation, *Angew. Chem., Int. Ed.*, 2013, **52**, 700–703.
31 S. M. Barnett, K. I. Goldberg and J. M. Mayer, A soluble copper–bipyridine water-oxidation electrocatalyst, *Nat. Chem.*, 2012, **4**, 498.
32 J. Du, Z. Chen, S. Ye, B. J. Wiley and T. J. Meyer, Copper as a Robust and Transparent Electrocatalyst for Water Oxidation, *Angew. Chem., Int. Ed.*, 2015, **54**, 2073–2078.
33 M.-T. Zhang, Z. Chen, P. Kang and T. J. Meyer, Electrocatalytic Water Oxidation with a Copper(II) Polypeptide Complex, *J. Am. Chem. Soc.*, 2013, **135**, 2048–2051.

34 T. Zhang, C. Wang, S. Liu, J.-L. Wang and W. Lin, A Biomimetic Copper Water Oxidation Catalyst with Low Overpotential, *J. Am. Chem. Soc.*, 2014, **136**, 273–281.
35 D. J. Sconyers and J. D. Blakemore, Electrodeposition behavior of homoleptic transition metal acetonitrile complexes interrogated with piezoelectric gravimetry, *Analyst*, 2020, **145**, 466–477.
36 D. Grujicic and B. Pesic, Electrodeposition of copper: the nucleation mechanisms, *Electrochim. Acta*, 2002, **47**, 2901–2912.
37 W. Lubitz, H. Ogata, O. Rüdiger and E. Reijerse, Hydrogenases, *Chem. Rev.*, 2014, **114**, 4081–4148.
38 J. Zhang, B. Xiao, X. Liu, P. Liu, P. Xi, W. Xiao, J. Ding, D. Gao and D. Xue, Copper dopants improved the hydrogen evolution activity of earth-abundant cobalt pyrite catalysts by activating the electrocatalytically inert sulfur sites, *J. Mater. Chem. A*, 2017, **5**, 17601–17608.
39 Q. Wu, M. Luo, J. Han, W. Peng, Y. Zhao, D. Chen, M. Peng, J. Liu, F. M. F. de Groot and Y. Tan, Identifying Electrocatalytic Sites of the Nanoporous Copper–Ruthenium Alloy for Hydrogen Evolution Reaction in Alkaline Electrolyte, *ACS Energy Lett.*, 2020, **5**, 192–199.
40 M. Kügler, J. Scholz, A. Kronz and I. Siewert, Copper complexes as catalyst precursors in the electrochemical hydrogen evolution reaction, *Dalton Trans.*, 2016, **45**, 6974–6982.
41 S. Cao, C.-J. Wang, G.-Q. Wang, Y. Chen, X.-J. Lv and W.-F. Fu, Visible light driven photo-reduction of Cu^{2+} to Cu_2O to Cu in water for photocatalytic hydrogen production, *RSC Adv.*, 2020, **10**, 5930–5937.
42 P. Zhang, M. Wang, Y. Yang, T. Yao and L. Sun, A Molecular Copper Catalyst for Electrochemical Water Reduction with a Large Hydrogen-Generation Rate Constant in Aqueous Solution, *Angew. Chem., Int. Ed.*, 2014, **53**, 13803–13807.
43 H. I. Karunadasa, E. Montalvo, Y. Sun, M. Majda, J. R. Long and C. J. Chang, A Molecular MoS_2 Edge Site Mimic for Catalytic Hydrogen Generation, *Science*, 2012, **335**, 698–702.
44 H. Lei, H. Fang, Y. Han, W. Lai, X. Fu and R. Cao, Reactivity and Mechanism Studies of Hydrogen Evolution Catalyzed by Copper Corroles, *ACS Catal.*, 2015, **5**, 5145–5153.
45 J.-P. Cao, T. Fang, L.-Z. Fu, L.-L. Zhou and S.-Z. Zhan, First mononuclear copper(II) electro-catalyst for catalyzing hydrogen evolution from acetic acid and water, *Int. J. Hydrogen Energy*, 2014, **39**, 13972–13978.
46 L.-Z. Fu, T. Fang, L.-L. Zhou and S.-Z. Zhan, A mononuclear copper electrocatalyst for both water reduction and oxidation, *RSC Adv.*, 2014, **4**, 53674–53680.
47 J.-P. Cao, T. Fang, Z.-Q. Wang, Y.-W. Ren and S. Zhan, A dinuclear triazenido–copper complex: A new molecular electro-catalyst for generating hydrogen from acetic acid or water, *J. Mol. Catal. A: Chem.*, 2014, **391**, 191–197.
48 J. Wang, C. Li, Q. Zhou, W. Wang, Y. Hou, B. Zhang and X. Wang, Photocatalytic hydrogen evolution by Cu(ii) complexes, *Dalton Trans.*, 2016, **45**, 5439–5443.
49 D. M. Ekanayake, K. M. Kulesa, J. Singh, K. K. Kpogo, S. Mazumder, H. Bernhard Schlegel and C. N. Verani, A pentadentate nitrogen-rich copper electrocatalyst for water reduction with pH-dependent molecular mechanisms, *Dalton Trans.*, 2017, **46**, 16812–16820.
50 Z.-J. Xin, S. Liu, C.-B. Li, Y.-J. Lei, D.-X. Xue, X.-W. Gao and H.-Y. Wang, Hydrogen production in a neutral aqueous solution with a water-soluble copper complex, *Int. J. Hydrogen Energy*, 2017, **42**, 4202–4207.
51 K. Majee, J. Patel, B. Das and S. K. Padhi, μ-Pyridine-bridged copper complex with robust proton-reducing ability, *Dalton Trans.*, 2017, **46**, 14869–14879.
52 T. Fang, H.-X. Lu, J.-X. Zhao, S.-Z. Zhan and Q.-Y. Lv, A new copper(I)–triazenido electro-catalyst for catalyzing hydrogen evolution from acetic acid and water, *J. Mol. Catal. A: Chem.*, 2015, **396**, 304–309.
53 T. Fang, L.-L. Zhou, L.-Z. Fu, S.-Z. Zhan and Q.-Y. Lv, Synthesis and studies of a molecular copper(I)-triazenido electrocatalyst for catalyzing hydrogen evolution from acetic acid and water, *Polyhedron*, 2015, **85**, 355–360.
54 M. J. Samide and D. G. Peters, Electrochemical reduction of copper(II) salen at carbon cathodes in dimethylformamide, *J. Electroanal. Chem.*, 1998, **443**, 95–102.
55 S. Kim, C. Saracini, M. A. Siegler, N. Drichko and K. D. Karlin, Coordination Chemistry and Reactivity of a Cupric Hydroperoxide Species Featuring a Proximal H-Bonding Substituent, *Inorg. Chem.*, 2012, **51**, 12603–12605.
56 K. D. Karlin, J. C. Hayes, S. Juen, J. P. Hutchinson and J. Zubieta, Tetragonal vs. trigonal coordination in copper (II) complexes with tripod ligands: structures and properties of $[Cu(C_{21}H_{24}N_4)Cl]PF_6$ and $[Cu(C_{18}H_{18}N_4)Cl]PF_6$, *Inorg. Chem.*, 1982, **21**, 4106–4108.
57 N. Kaeffer, A. Morozan, J. Fize, E. Martinez, L. Guetaz and V. Artero, The Dark Side of Molecular Catalysis: Diimine–Dioxime Cobalt Complexes Are Not the Actual Hydrogen Evolution Electrocatalyst in Acidic Aqueous Solutions, *ACS Catal.*, 2016, **6**, 3727–3737.
58 K. J. Lee, B. D. McCarthy and J. L. Dempsey, On decomposition, degradation, and voltammetric deviation: the electrochemist's field guide to identifying precatalyst transformation, *Chem. Soc. Rev.*, 2019, **48**, 2927–2945.
59 R. Sanyal, S. A. Cameron and S. Brooker, Synthesis and complexes of an N_4 Schiff-base macrocycle derived from 2,2′-iminobisbenzaldehyde, *Dalton Trans.*, 2011, **40**, 12277–12287.
60 R. K. Wilson and S. Brooker, Complexes of a porphyrin-like N_4-donor Schiff-base macrocycle, *Dalton Trans.*, 2013, **42**, 7913–7923.
61 I. M. Procter, B. J. Hathaway and P. Nicholls, The electronic properties and stereochemistry of the copper(II) ion. Part I. Bis(ethylenediamine)copper(II) complexes, *J. Chem. Soc. A*, 1968, 1678–1684.
62 B. J. Hathaway and D. E. Billing, The electronic properties and stereochemistry of mono-nuclear complexes of the copper(II) ion, *Coord. Chem. Rev.*, 1970, **5**, 143–207.
63 I. M. Procter, B. J. Hathaway and P. G. Hodgson, The electronic properties and stereochemistry of the copper(II) ion

—V^{III}: Mono(ethylenediamine)- and mono(2,2′-bipyridyl)-copper(II) complexes, *J. Inorg. Nucl. Chem.*, 1972, **34**, 3689–3697.

64 L. Yang, D. R. Powell and R. P. Houser, Structural variation in copper(I) complexes with pyridylmethylamide ligands: structural analysis with a new four-coordinate geometry index, τ4, *Dalton Trans.*, 2007, 955–964.

65 A. W. Addison, T. N. Rao, J. Reedijk, J. van Rijn and G. C. Vershoor, Synthesis, structure and spectroscopic properties of copper(II) compounds containing nitrogen-sulphur donor ligands; the crystal and molecular structure of aqua[1,7-bis(N-methylbenzimidazol-2′-yl)2,6-dithiaheptane]copper(II) perchlorate, *Dalton Trans.*, 1984, 1349–1356.

66 A. Das, Z. Han, W. W. Brennessel, P. L. Holland and R. Eisenberg, Nickel Complexes for Robust Light-Driven and Electrocatalytic Hydrogen Production from Water, *ACS Catal.*, 2015, **5**, 1397–1406.

67 R. S. Khnayzer, V. S. Thoi, M. Nippe, A. E. King, J. W. Jurss, N. Roz, K. A. El, J. R. Long, C. J. Chang and F. N. Castellano, Towards a comprehensive understanding of visible-light photogeneration of hydrogen from water using cobalt(II) polypyridyl catalysts, *Energy Environ. Sci.*, 2014, **7**, 1477–1488.

68 F. Lucarini, M. Pastore, S. Vasylevskyi, M. Varisco, E. Solari, A. Crochet, K. M. Fromm, F. Zobi and A. Ruggi, Heptacoordinate Co^{II} complex: a new architecture for photochemical H_2 production, *Chem. – Eur. J.*, 2017, **23**, 6768–6771.

69 Y. Kuramochi and O. Ishitani, Iridium(III) 1-Phenylisoquinoline Complexes as a Photosensitizer for Photocatalytic CO_2 Reduction: A Mixed System with a Re(I) Catalyst and a Supramolecular Photocatalyst, *Inorg. Chem.*, 2016, **55**, 5702–5709.

70 S. Chakraborty, E. H. Edwards, B. Kandemir and K. L. Bren, Photochemical Hydrogen Evolution from Neutral Water with a Cobalt Metallopeptide Catalyst, *Inorg. Chem.*, 2019, **58**, 16402–16410.

71 N. Elgrishi, K. J. Rountree, B. D. McCarthy, E. S. Rountree, T. T. Eisenhart and J. L. Dempsey, A Practical Beginner's Guide to Cyclic Voltammetry, *J. Chem. Educ.*, 2018, **95**, 197–206.

72 P. Zanello, *Inorganic Electrochemistry: Theory, Practice and Application*, Royal Society of Chemistry, Cambridge, UK, 2003.

73 S. Nestke, E. Ronge and I. Siewert, Electrochemical water oxidation using a copper complex, *Dalton Trans.*, 2018, **47**, 10737–10741.

74 B. D. McCarthy, D. J. Martin, E. S. Rountree, A. C. Ullman and J. L. Dempsey, Electrochemical reduction of Brønsted acids by glassy carbon in acetonitrile—implications for electrocatalytic hydrogen evolution, *Inorg. Chem.*, 2014, **53**, 8350–8361.

75 V. Fourmond, P.-A. Jacques, M. Fontecave and V. Artero, H_2 Evolution and Molecular Electrocatalysts: Determination of Overpotentials and Effect of Homoconjugation, *Inorg. Chem.*, 2010, **49**, 10338–10347.

76 K. Izutsu, *Acid-Base Dissociation Constants in Dipolar Aprotic Solvents*, 1990.

77 L. Tong, L. Duan, A. Zhou and R. P. Thummel, First-row transition metal polypyridine complexes that catalyze proton to hydrogen reduction, *Coord. Chem. Rev.*, 2020, **402**, 213079.

78 M. L. Helm, M. P. Stewart, R. M. Bullock, M. R. DuBois and D. L. DuBois, A Synthetic Nickel Electrocatalyst with a Turnover Frequency Above 100,000 s^{-1} for H_2 Production, *Science*, 2011, **333**, 863–866.

79 A. M. Appel and M. L. Helm, Determining the Overpotential for a Molecular Electrocatalyst, *ACS Catal.*, 2014, **4**, 630–633.

80 E. S. Rountree, B. D. McCarthy, T. T. Eisenhart and J. L. Dempsey, Evaluation of Homogeneous Electrocatalysts by Cyclic Voltammetry, *Inorg. Chem.*, 2014, **53**, 9983–10002.

81 M. Rakowski DuBois and D. L. DuBois, The roles of the first and second coordination spheres in the design of molecular catalysts for H2 production and oxidation, *Chem. Soc. Rev.*, 2009, **38**, 62–72.

82 D. K. Bediako, B. H. Solis, D. K. Dogutan, M. M. Roubelakis, A. G. Maher, C. H. Lee, M. B. Chambers, S. Hammes-Schiffer and D. G. Nocera, Role of pendant proton relays and proton-coupled electron transfer on the hydrogen evolution reaction by nickel hangman porphyrins, *Proc. Natl. Acad. Sci. U. S. A.*, 2014, **111**, 15001–15006.

83 R. M. Bullock and M. L. Helm, Molecular electrocatalysts for oxidation of hydrogen using earth-abundant metals: shoving protons around with proton relays, *Acc. Chem. Res.*, 2015, **48**, 2017–2026.

84 A. D. Wilson, R. H. Newell, M. J. McNevin, J. T. Muckerman, M. Rakowski DuBois and D. L. DuBois, Hydrogen Oxidation and Production Using Nickel-Based Molecular Catalysts with Positioned Proton Relays, *J. Am. Chem. Soc.*, 2006, **128**, 358–366.

85 X. L. Ho, H. Shao, Y. Y. Ng, R. Ganguly, Y. Lu and H. S. Soo, Visible Light Driven Hydrogen Evolution by Molecular Nickel Catalysts with Time-Resolved Spectroscopic and DFT Insights, *Inorg. Chem.*, 2019, **58**, 1469–1480.

86 R. K. Wilson and S. Brooker, Oxidative dehydrogenation of a new tetra-amine N_4-donor macrocycle tunes the nickel(II) spin state from high spin to low spin, *Dalton Trans.*, 2013, **42**, 12075–12078.